Tailoring the Surface Functionalities of Titania Nanotubes for Biomedical Applications

V. S. Simi, L. Mohan, and N. Rajendran

Abstract Self-organized vertically aligned nanostructures grown on metallic substrates via anodization have attracted significant scientific attention for a wide range of applications. These nanotubular structures integrate highly controllable geometry at the nanoscale with fascinating biological and mechanical properties. This chapter attempts to cover the key electrochemical factors that control the tube geometry and also demonstrate various surface functionalization approaches for modifying the surface properties of TiO_2 nanotubes to develop new and pioneering functional biomaterials for biomedical applications. Furthermore, the anodization parameters that have led to the formation of nanotubes on various titanium alloys were also discussed.

Keywords Titania nanotubes · Anodization · Functionalization · Biocompatibility

1 Introduction

A biomaterial is any matter or surface derived either from nature or synthesized in the laboratory that interacts with the biological systems. They are often used or adapted for a medical application, encompassing a part or whole of a living structure or a designed medical device that performs, augments, or replaces a natural function [1].

V. S. Simi
Department of Applied Science, Sree Chitra Thirunal College of Engineering, Trivandrum, Kerala, India

V. S. Simi (✉) · N. Rajendran
Department of Chemistry, CEG, Guindy Campus, Anna University, Chennai, Tamil Nadu, India
e-mail: simisasidharan08@gmail.com

N. Rajendran
e-mail: nrajendran@annauniv.edu

L. Mohan
Department of Mechanical Engineering, Toyohashi University of Technology, Toyohashi, Japan

T. S. Santra and L. Mohan (eds.), *Nanomaterials and Their Biomedical Applications*, Springer Series in Biomaterials Science and Engineering 16,
https://doi.org/10.1007/978-981-33-6252-9_17

Biomaterials and medical devices have evolved over the last 50 (or) so years to a $100 billion endeavor [2]. From the past few decades, due to the increase in the participation of many persons in defense activities, sports, utilization of self-operating machines, and increased interest in motorcycles has resulted in enormous increase in the number of accidents, which necessarily led people to opt for orthopaedic implants [3].

In orthopaedics, the biomaterial devices used are commonly called as implants and are manufactured for a great number in orthopaedic applications. An adequate level of tolerance of the material with the living organism i.e. biocompatibility is essential to successfully apply an implant in the human body. Despite the success of traditional materials, new and innovative biomaterials are being developed continuously to satisfy the ever increasing demands.

2 Material Choice for Biomedical Implants

The selection of suitable materials for orthopaedic implants relies on the specific applications. The material used as an implant should have the desired balance of both physical and mechanical properties necessary to perform as expected in the human body. Also, the device should be relatively easy to fabricate, consistent, reproducible, and confirm to all technical and biological requirements [4]. Over the past few decades, a wide range of materials such as metals, ceramics, polymers, composites and biologically derived materials are commonly used in orthopaedic implants as the different physical, chemical, and biological properties that these materials possess can cater to specific applications [5–9]. While traditional materials such as stainless steel, Co-based alloys, Titanium and its alloys are constantly modified to be more effective biomaterials, resulting in improved medical devices, new materials continued to be explored as alternatives [10].

3 Titanium-Based Biomaterials

In the current scenario, titanium and its alloys are extensively used in biomedical field and have a good record of being used as a successful implant material due to the metal's exceptional properties. Titanium- based biomaterials are inert and proven to be superior in terms of biocompatibility and corrosion resistance than Co-Cr and stainless steel alloys, hence becoming the material choice by most of the clinicians, material scientist, surgeons and medical device designers [11]. The implant applications of titanium included replacement of hard tissue in artificial bones, joints, cardiovascular implants like prosthetic heart valves, pacemaker cases, circulatory devices, dental implants, screws and staples for spinal surgery [12]. They are preferred materials for load- bearing and long term implants and reveal high mechanical properties and biocompatibility. However, they are bio inert, thus could not directly bond to living bone tissues [13, 14].

4 Surface Modification for Titanium Implants

The selection of right biomaterial for a specific biomedical application relies on the bulk properties of biomaterial such as corrosion resistance, non-toxicity, controlled degradability, modulus of elasticity and fatigue strength. After implantation, a sequence of local events such as classic foreign body response and fibrous tissue capsule formation occurs around the implant [15]. The biomaterial surface act as a major influencing factor for the above said unfavorable reactions of the body, as the initial contact of the body is with the surface [16]. Despite many advantageous properties, Ti-based alloys are poor in bioactivity, as they cannot bond directly with bone due to fibrous encapsulation and promote new bone formation on the surface at the initial stage after implantation [17]. Successful implantation of titanium implants lies in demonstrating excellent osseointegration at the bone-implant surface and hence it is essential to improve the tissue bonding properties of titanium implants. The schematic representation of the successful implantation procedure is shown in Fig. 1(A). The direct contact between the bone and implant Fig. 1(A)–c is essential for successful implantation procedure. The formation of fibrous tissue can start a vicious cycle of micromotion and inflammation around the implant surface, which isolates implanted material from the surrounding bone and finally leads to implant failure [18, 19].

The surface chemistry and structure of the material are the two essential factors determining the interactions of the material with the neighboring tissue. Also, it is evident that the extend of osseointegration and the response of titanium-based biomaterials depend entirely on its biocompatibility and surface properties [21]. Hence various surface modifications such as mechanical, physical, chemical, electrochemical or biochemical modifications [22–31] are considered at improving the osseointegration property of the implant surface. The proper surface modification method not only retains the excellent bulk features of titanium and its alloys, but also improves specific surface properties required for diverse clinical applications [27].

5 Nanoscale Surface Modification-Formation of TiO_2 Nanotubes

The exploit of nanostructured materials has been proposed to resolve some of the problems presently associated with implants. As the modified coated surfaces obtained from various surface modification techniques are not reliable for long period due to the relatively higher micrometer level thickness and poor adhesion of the coated layer to the substrate [32], fracture and delamination occur at the bone-implant interface. The length scale of the hierarchical structure of the tissue must be considered, while designing a synthetic material which is intended to efficaciously replace living tissue in an organism [33]. The whole length scale from the nanoscale up to macroscale needs to be taken into account. The interactions between the bone

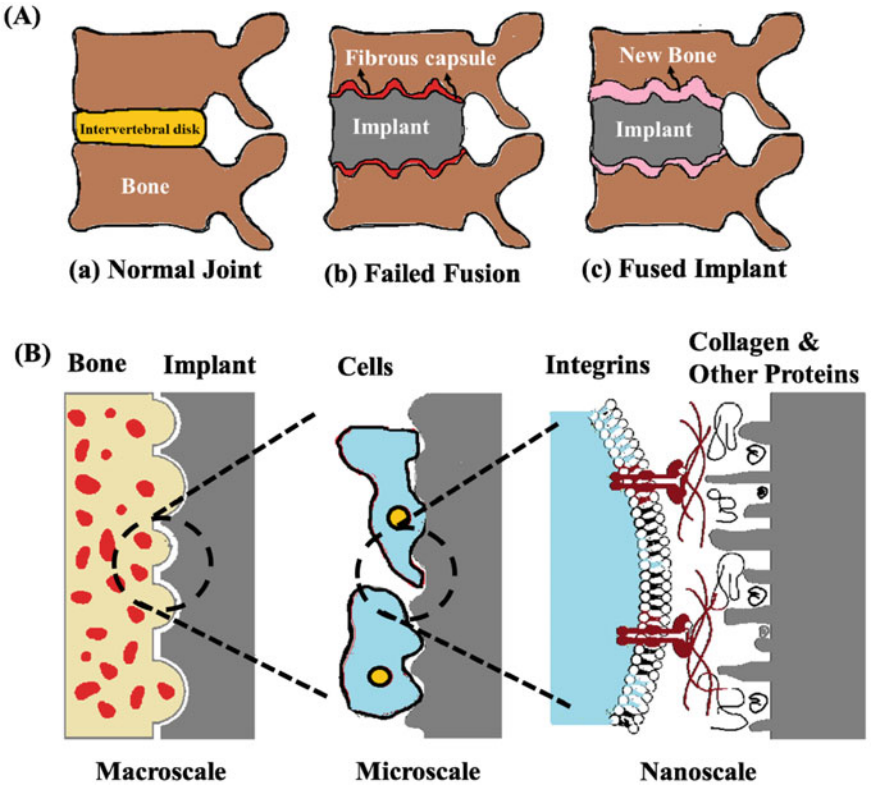

Fig. 1 (A) Schematic representation of (a) a normal joint, (b) a failed implant and (c) a fused and osseointegrated implant. (B) Interactions between the bone and the implant surface at different length scales (macro, micro and nano) (Redrawn from ref [15, 20])

and the implant surface at different length scales are shown in Fig. 1(B). The implant should provide a good mechanical fixation with bone at the macroscale. The micro- and submicro features presented on the surface can directly interact with osteoblasts and mesenchymal stem cells at the microscale. At the nanoscale, cell membrane receptors, such as integrins, can identify proteins adsorbed on the surface, which in turn are controlled by the nanostructures on the surface [15]. At the initial level, bone has a structural hierarchy in the nanometer regime and hence nanostructured materials are believed to play a vibrant role in orthopaedic research [34]. Modifying Ti surfaces with the formation of self-organized TiO_2 nanotubes enhances bone-bonding characteristics than conventional micro roughened surfaces. Altering the surface morphology of the titanium to nanoscale by forming nanotube structures can enhance the surface properties of titanium [35–37]. Also, the large surface area provided by the nanostructured topography renders available sites for the adsorption of protein and thus improves the cell-implant interactions [38]. Additionally,

the structural modification at the nanoscale would mimic the nanostructure of the natural bone and hence favor a positive cellular interaction with cells [39].

Synthesis of titania nanostructures can be achieved by various routes including template–assisted methods [40, 41], hydro/solvothermal approaches [42, 43], Sol-gel method [44, 45] and by electrochemical method [46, 47]. Among all these methods, anodization, a relatively inexpensive and scalable electrochemical process is widely used for the growth of most spectacular, self-organized 1D nanotube structures. These nanotubular structures integrate highly controllable geometry at the nanoscale fascinating chemical and biological properties [48].

6 Formation Mechanism of TiO_2 Nanotubes

Figure 2 illustrates a typical two-electrode set up for the anodization of Ti substrates. The metallic Ti/alloy and platinum were used as anode and cathode respectively in the construction of electrochemical cell. The direct current generated by a DC power source in this case, drives the anodization process. The electrolyte temperature, pH

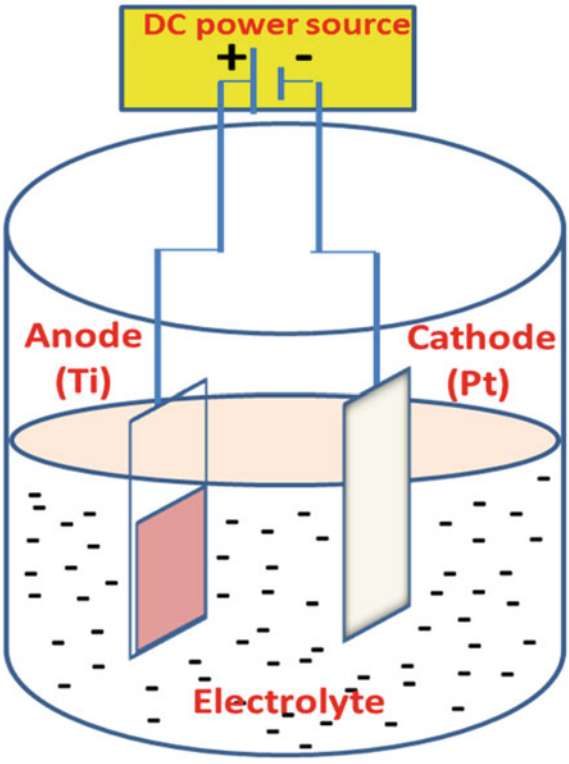

Fig. 2 Schematic representation of anodization cell

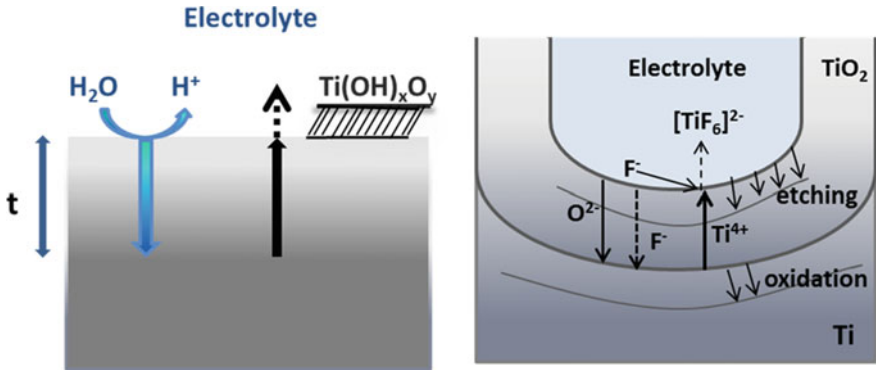

Fig. 3 Schematic representation of the Ti anodization (a) in absence of fluorides (results in flat layers), and (b) in presence of fluorides (results in the tube growth) (Redrawn from [48])

and real-time circuit potential and current can be measured during the growth of metallic oxide layer.

The chemistry that dictates the formation of nanotubes includes the interactions of the three competing reactions i.e. (i) field-assisted oxidation at the metal surface (ii) field-assisted dissolution of Ti metal to form titanium dioxide and (iii) chemical dissolution of generated oxide layer due to the etching by fluorides present in the electrolyte [48, 49].

Initially, the anodization process generates a stable TiO_2 layer of thickness 't' due to the transport of oxide and metallic ions across the oxide layer. When the electrochemical conditions are optimized and a chemical etching source such as fluoride compound is integrated into the electrolyte, field-assisted dissolution of the transported metallic ions and chemical dissolution of oxide layer takes place and this lead to the formation of porous (or) tubular layer [50, 51]. The schematic representation of the Ti anodization in the presence and absence of fluorides is shown in Fig. 3.

The following Eqs. (1) and (2), (3) represents the oxide layer formation and dissolution reactions respectively. The reactions described by Eqs. (1)–(3) subsequently compete with one another leading to the deepening of the pores as a high electric field is located at the bottom of the pore compared with the tube wall [52]. Finally, due to the growth of smaller pits at the inter-pore region, vertical tubes start to form and ultimately lead to the generation of a tubular structure.

$$Ti + 2H_2O \rightarrow TiO_2 + 4H^+ + 4e^- \quad (1)$$

$$TiO_2 + 6F^- + 4H^+ \rightarrow [TiF_6]^{2-} + H_2O \quad (2)$$

$$Ti^{4+} + 6F^- \rightarrow [TiF_6]^{2-} \quad (3)$$

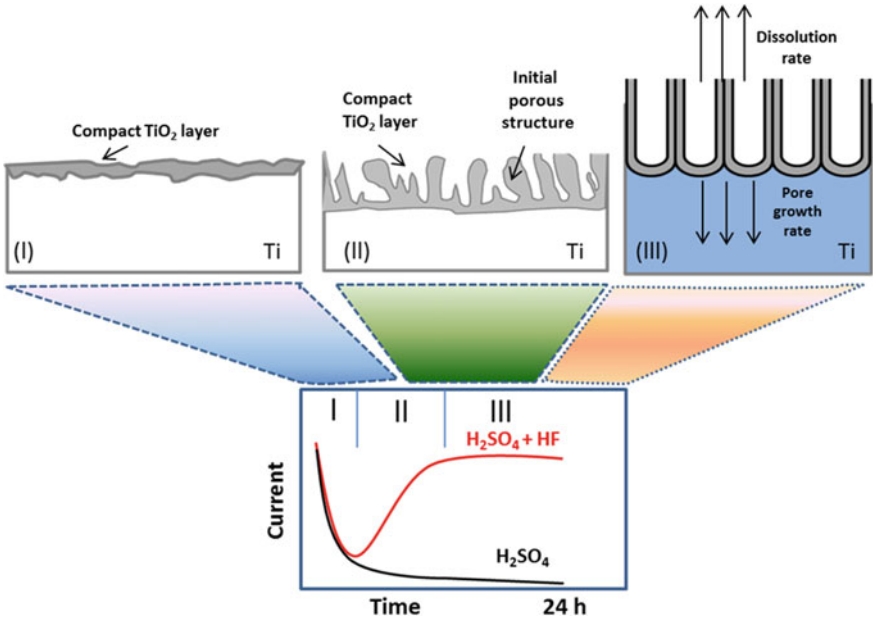

Fig. 4 Characteristic current-time plot for anodization of Ti substrates with and without fluorides in the electrolyte and the evolution of corresponding surface morphology in electrolytes containing fluorides (Redrawn from [48])

A typical anodization current—time plot that develops a nanotube layer is represented in Fig. 4. The formation of nanotubes can be related to main three key phases of current—time plot. In Fig. 4, an initial decrease in the current over time (stage I) observed, is due to the oxide layer formation on the surface. Further, a decrease in electric field strength is observed as represented in the figure in the absence of a chemical etching agent in the electrolyte. In the presence of electrolyte, the initial decay period (phase I) is followed by an increase in current, indicates the interactions of reactions (i), (ii) and (iii) mentioned above and this results in the formation of a porous structure. Finally, at stage III, an equilibrium is attained between the rate of oxide formation and dissolution reactions and as a result, the current value attains a steady state due to the formation of nanotubes [51].

7 Factors Influencing the Growth of Nanotube Layers

7.1 Effect of Anodization Voltage

In electrochemical anodization, applied potential plays an essential role in modifying the topography of nanotube structures. The applied anodization potential influences

the electric field strength experienced across the formed oxide and thus affecting the ions migration and ultimately the diameter of the nanotubes [53]. A linear relationship exists between the diameter and the applied potential [54] and also to the thickness of the barrier layer at the base of the nanotubes [55]. The potential applied has a direct effect on the rates of oxidation and dissolution reactions that takes place during the nanotube formation. Cai et al. [56] reported that the nanotube diameter, at the tube mouth and bottom are directly proportional to the applied potential. It was also mentioned that anodically grown nanotubular layers will only be generated, if the applied potential is kept within the range dictated by the chemical dissolution activity of the electrolyte. If the potential is too low, the induced rates of oxidation and dissolution occur too slowly relative to the chemical etching performed by the electrolyte, leading to the formation of pits and not the oxide layer. If the potential is too high, field-assisted oxidation occurs too quickly relative to the chemical dissolution of the metallic substrate, which results in the formation of disturbed oxide layer rather than the nanotubular layer [57]. Sulka et al. [58] extensively studied the influence of anodizing potential on the structural parameters of porous anodic titania including pore diameter, inter pore distance, wall thickness, porosity and pore density.

To study the effect of applied voltage on the morphology of TiO_2 nanotubes, Ti substrate was anodized in an electrolyte of glycerol with 1 weight % NH_4F and 20 volume % water for 1 h at different voltages (10, 20 and 30 V) [59]. Figure 5 shows the HR-SEM images and the corresponding 3D images of the formed nanotubes at different voltages. The influence of applied electric field in the formation of nanotubes with varying diameter was visible from the HR-SEM (Fig. 5) images.

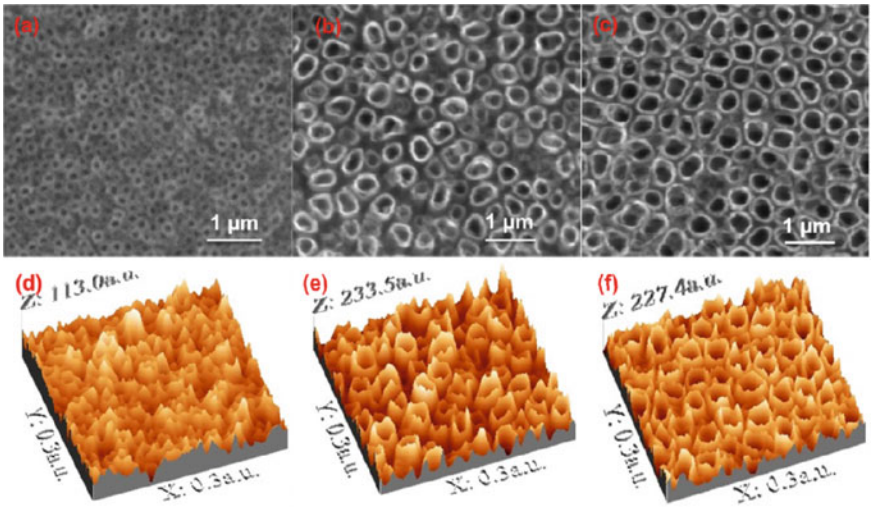

Fig. 5 HR-SEM images (top view) and corresponding 3D images of Ti specimen anodized at different voltages (a, d) 10 V (b, e) 20 V and (c, f) 30 V (Adapted from [59])

Samples anodized at 10 V exhibits a porous morphology with average diameter 32 nm. No inter-tubular space was observed. Regular and self-organized nanotubes with diameter approximately 45 and 58 nm for the titanium substrate anodized at 20 and 30 V respectively were observed. Nanotubes were separated with inter-tubular spaces and the height of the nanotubes was found to be 540 nm.

The influence of potential in the formation of nanotubes in the anodization of Ti-6Al-7Nb alloy was also studied [19]. The FESEM images of titania nanotubes obtained by anodisation of Ti-6Al-7Nb for 1 h in an electrolyte consisting of 1 M H_2SO_4 and 0.08 M HF at different voltages 10, 20 and 30 V are shown in Fig. 6a, c and e. Sample anodized at 10 V show a nanoporous morphology with a diameter of 35 nm and height 250 nm. Moreover, no inter-tubular space and wall separation was observed at this voltage. TNT anodized at 20 and 30 V show a very regular and vertically aligned tubular structure as shown in the FESEM images. Similarly, the 3D image of the TiO_2 nanotube array generated from FESEM image for the same from higher magnification are given in Fig. 6b, d and f.

The tubular morphology formed on Ti-6Al-7Nb alloy resembles well-known as in the case of nanotubes obtained on pure Ti foils. Also, the 2D profile of the TiO_2 nanotube layer generated from FESEM image is demonstrated in Fig. 7. These studies

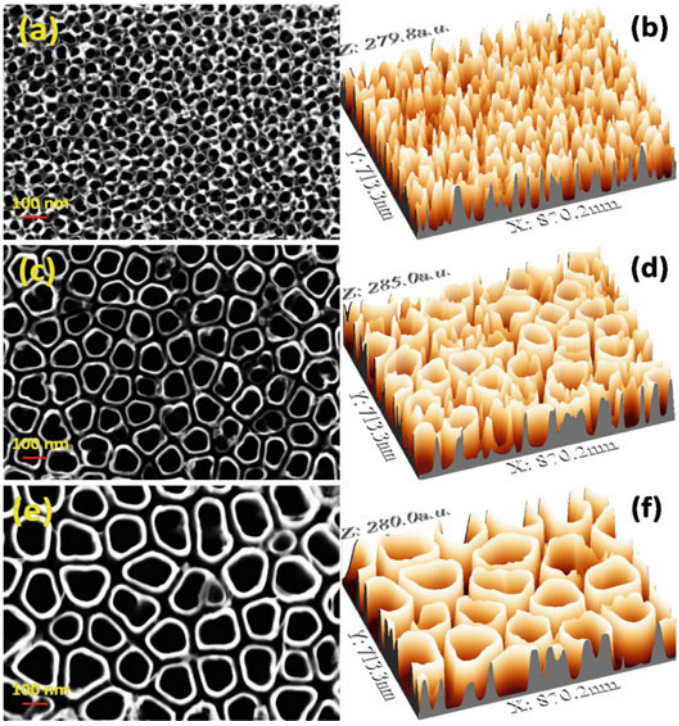

Fig. 6 FESEM images of TiO_2 nano tubes (left) and 3D images (right) for 10 V (a and b), 20 V (c and d) and 30 V (e and f) (Reprinted with permission from [19])

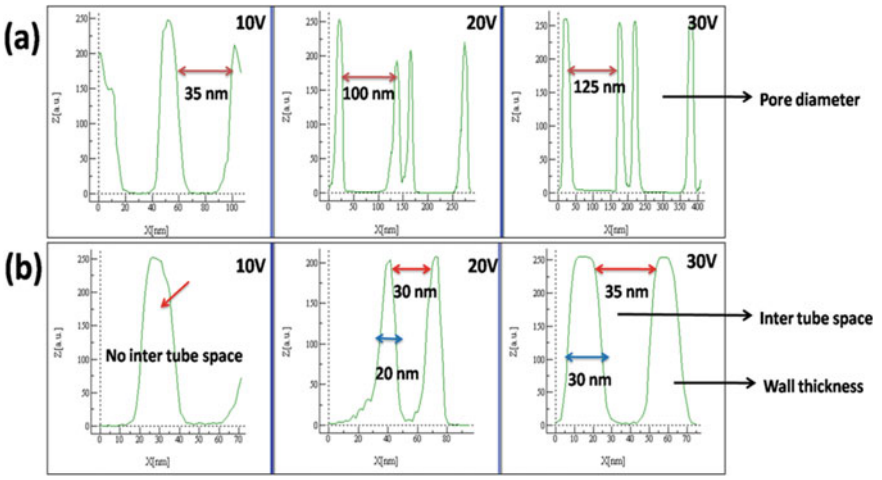

Fig. 7 2D profile of TNTs at 10, 20 and 30 V; **a** pore diameter, **b** inter tube space and wall thickness (Reprinted with permission from [19])

indicate that the pore diameter increases with increase in voltage which is in line with earlier reports on pure titanium.

7.2 Effect of Anodization Time

During anodization the key factor which controls the morphology of nanostructures is anodization time. In general, identification of critical point is important for the formation of nanotubes. It has been reported that this critical points occurred within 2–3 min after the initiation of anodization process in the case of 0.5 M HF electrolyte. It is important to give enough time for nanotube nucleation to takes place on the substrate surface [48]. As the anodization duration increases, the thickness of the oxide layer increases. Also, there is an increase in tube length with time, until an equilibrium reached between the formation and dissolution of titanium oxide. After this point, the nanotube length becomes independent of anodizing time [60].

It was believed that anodization time influences the tubular morphology. Figure 8 shows TiO_2 nanotubes fabricated at different times in Ti-6Al-7Nb alloy. The substantial role of anodization time for the transformation of pores to tubes was demonstrated by Mohan et al. [61] by the anodization of Ti-6Al-7Nb alloy in an electrolyte made by mixing 50 ml of 0.08 M HF in 50 ml of 1 M sulphuric acid. The color of the titanium oxide layer turned from dark purple to blue, yellow and finally to greenish-blue during this period. The change in color of the titanium oxide is due to the increase in the thickness of the oxide layer which results in interference of light.

The current-time transient curve for Ti-6Al-7Nb anodized at a different time at 30 V is given in Fig. 9. The authors explained that the initial drop in current is

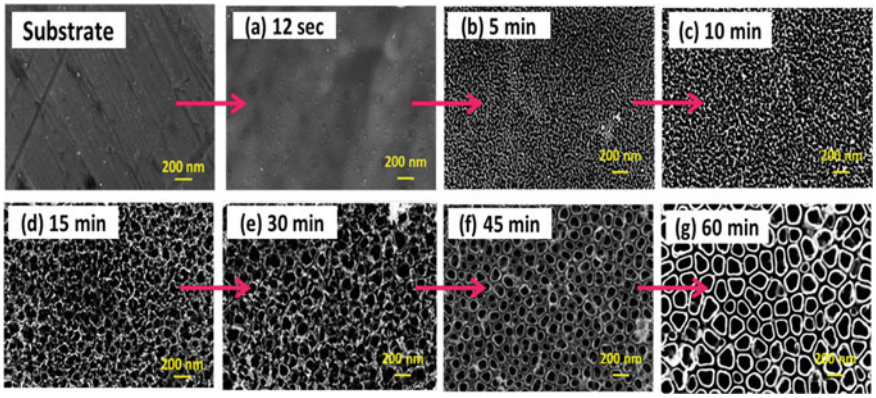

Fig. 8 FESEM images of Ti-6Al-7Nb anodized at different time **a** 12 s, **b** 5 min, **c** 10 min, **d** 15 min, **e** 30 min, **f** 45 min and **g** 60 min (Adapted and reprinted with permission from [61])

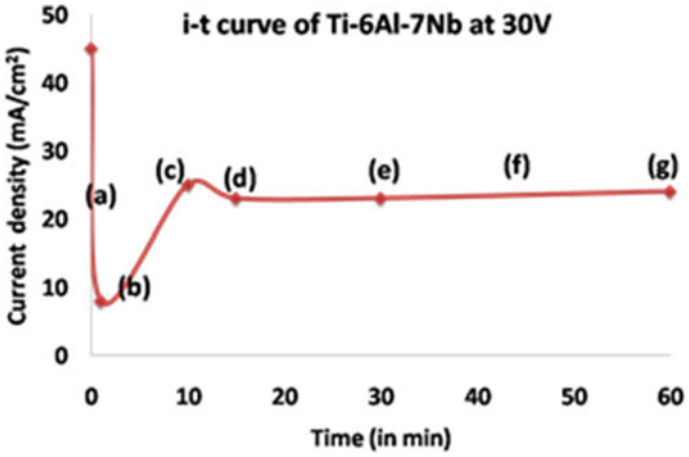

Fig. 9 Current-time transient curve for Ti-6Al-7Nb anodized at different time at 30 V (Reprinted with permission from [61])

due to oxide formation and subsequent increase in the corrosion current due the development of porous structure due to the dissolution of oxide layer by fluoride (F^-) ions. Finally, the current reaches a steady-state with the steady growth of the TiO_2 nanotubes. It was demonstrated that, the conversion of oxide layer to a tubular structure begins when the corrosion current starts to decrease.

In aqueous electrolyte, the aggressive condition does not allow the nanotubes to grow longer than a few μm [56, 62]. However, the anodization usually carried out from 30 min to 2 h for structural rearrangement and thereby increase the degree of self-ordering [63]. In the case of organic electrolyte, the growth process is slower and dissolution phenomena are not as significant as it occurs in water. Hence it was

possible to obtain nanotubes over 100 μm by extending the anodization time [64]. However, the length of the nanotubes has no noteworthy influence on the biocompatibility of nanotubes as the cells contact initially on the upper surface of the tubular structure. On the other side, it was reported that the tube length has a great effect on drug release rate which can be controlled by tuning the aspect ratio of the nanotubes [65].

7.3 Effect of Electrolyte Composition

The nanostructures are usually formed by a variety of fluoride-containing aqueous [51, 66] or organic [67, 68] electrolyte by anodizing titanium at different voltages. It has been reported that the geometry of the formed nanotubes has a direct influence on the basic electrolyte parameters such as pH, fluoride ion concentration temperature and water content [48, 61, 69]. The fluoride ion concentration in the electrolyte has an important role in the self-ordering of nanotubes. The fluoride concentration should be minimum and sufficient to ensure the growth of nanotubes. The studies have shown that the typical F^- concentration leading to the self-ordering of nanotubes is in the range of 0.3–0.5 wt% [70, 71]. The presence of fluoride ions in the electrolyte selectively etches the surface of titanium during the growth of oxide layer, which allows the formation of nanotubes. An increase in the concentration of fluoride ions obtained from the addition of HF or NH_4F increases nanotube diameter and length [72]. The influence of fluoride ion concentration in two different electrolytes 1 M $(NH_4)_2SO_4$ and 1 M Na_2SO_4 on TiO_2 nanotubes was reported. Nanotubes grown in organic electrolyte tend to be longer, homogenous and have smoother walls as the chemical dissolution and fluoride ion transmission rate is relatively low in viscous organic electrolytes [73, 74].

The water content in the electrolyte plays a vital role in the formation of titania nanotubes. Water content, the source of oxygen in most electrolytes is used to generate the initial oxide layer and has been reported to have a direct effect on nanotube wall thickness and length [48]. Raja et al. [75] reported that, to generate nanotube arrays on titanium, a minimum water content of 0.18 wt% is necessary in an electrolyte containing NH_4F and ethylene glycol. Mohammed et al. [76] reported that, an increase in nanotube diameter, wall thickness and length, when the water content increases up to 30% in an HH_4F containing electrolyte at a constant potential of 20 V. Various studies [62, 70, 77] reported that the nanotubes formed from low water content electrolyte results in smooth tube walls, whereas side wall ripples are formed at higher water content. This could be attributed to the faster etching of the fluoride-rich layer between the tubes than the growth speed of the tubes into the underlying substrate.

To evaluate this aspect, the water content in the electrolyte was varied by holding the anodization voltage and anodization time to 20 V and 1 h respectively [69]. A mixed solution of glycerol and ammonium fluoride with different water contents 10, 20 and 40 volume % was used as the electrolyte. The obtained nanotubes were

designated as TNTA-10, TNTA-20 and TNTA-40 respectively. The HR-SEM images of titania nanotubes formed in glycerol, ammonium fluoride electrolyte with different water contents, its cross- sectional view and the corresponding 3D images of the nanotubes generated from the HR-SEM images are given in Fig. 10a–l.

By varying the addition of water content into the electrolyte during the anodization process, the diameter of the nanotubes can be tuned. The morphology of the nanotubes formed in electrolyte with 1 volume % of water (TNTA-1) was given for comparison, despite the scanty reports available on the surface morphology of nanotubes formed at a low percentage of water content. It was observed that, irregular nanotubes with non-uniform diameter (Fig. 10a–c) were formed on titanium at lower water content.

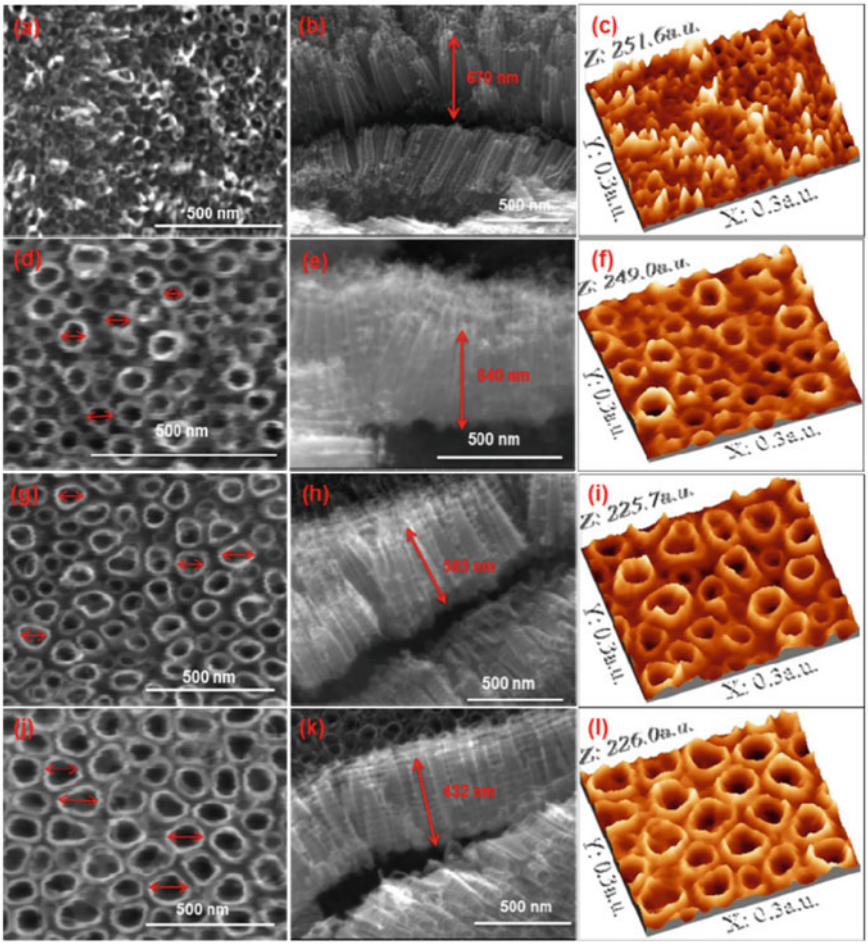

Fig. 10 HR-SEM images of titania nanotube arrays (top view) (left), cross-sectional view (middle) and 3D images (right) for (a, b, c) TNTA -1, (d, e, f) TNTA -10, (g, h, i) TNTA -20 and (j, k, l) TNTA -40 specimens (Reprinted with permission from [69])

As the water content increases, nanotube length was found to decrease and diameter of the nanotubes increases as evidenced from the HR-SEM images. It was apparent that, increasing water content increases the self-organization behavior of formed nanotubes. Highly self- organized nanotube structures were observed in TNTA-40, with higher water content. The formation of nanotubes with a varying diameter in electrolyte with different amounts of water is schematically represented in Fig. 11.

The diameter obtained for TNTA-1, TNTA-10, TNTA-20 and TNTA-40 specimens were found to be approximately 14, 30, 40 and 60 nm respectively. Intertubular spaces were observed between the nanotubes formed at high water content as evident from HR-SEM and 3D images. It is well-known that, controlling the tube features especially the nanotube diameter and inter tubular spacing supports the adhesion, proliferation and mineralization of cells [60]. Even after the cell adhesion, diameter and spacing between the nanotubes offers an important path for the continuous

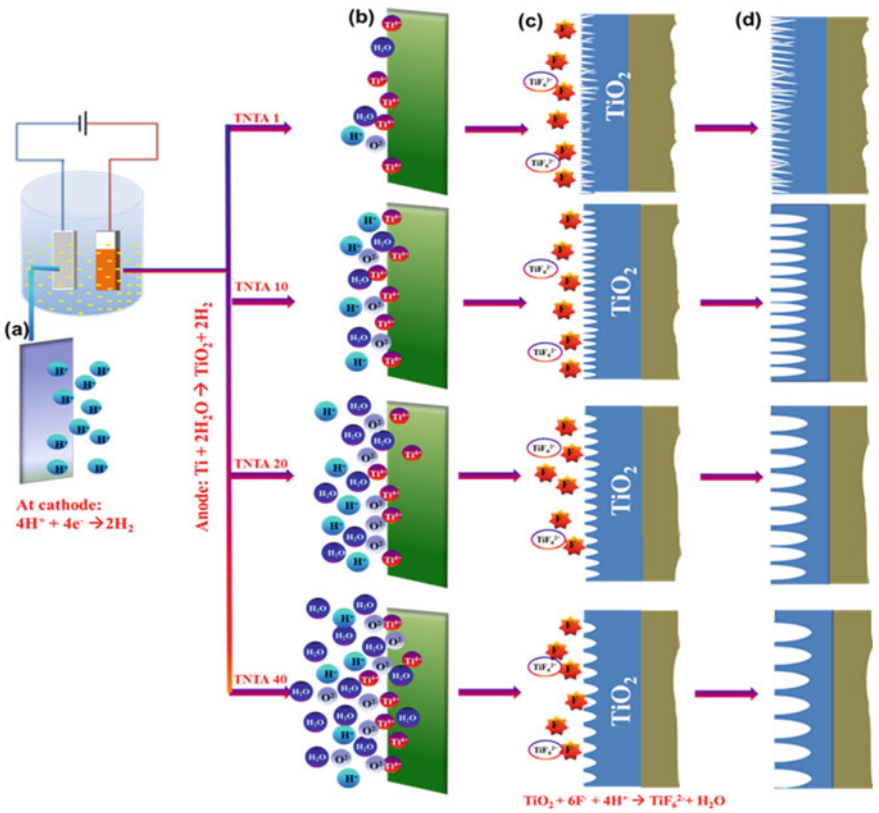

Fig. 11 Schematic diagram of nanotube formation **a** Cathodic reaction. **b** Anodic reaction. **c** Initiation of nanotube formation. **d** Formed nanotubes with different diameter (Reprinted with permission from [69])

fluid flow of culture media, ions, proteins, nutrients essential for healthy cell growth, increase spaces for the exchange of gas and cell signaling molecules for an overall improved cell environment. In human body, due to circulation and repetitive loading and unloading of bones during various activities, the fluid flow naturally occurs in the interstitial spaces around the bone cells [78–80].

7.4 Effect of Electrolyte Temperature

Another important parameter that influences the growth of nanotubes is anodization temperature. In most of the anodization process, the electrolytes are kept at room temperature to produce the nanotubes. It has been reported that an increase in electrolyte temperature leads to the formation of nanotubes with a larger diameter, shorter length and thinner walls [48]. The dissolution rates of the nanotubes are affected by the electrolyte temperature [53]. Prida et al. [81] reported that the growth of nanotubes is inhibited at lower temperatures (2 °C) in aqueous electrolyte, whereas the temperature range between 0 and 40 °C are reported to be most favorable for the growth of nanotubes in organic electrolyte [62]. Wang et al. [82] reported that the diameter of the nanotubes does not depend on the anodizing temperature in aqueous electrolyte, whereas the nanotube diameter was found to increase at higher temperatures while using in organic electrolyte. This could be due to the fact that at lower temperatures, the viscosity increases, which reduces the ion migration especially fluoride ion and as a result of which etching of TiO_2 gets slowed down, leading to smaller diameter tubes.

The influence of electrolyte temperature during the anodization of Ti-6Al-7Nb alloy was studied and reported [61]. Figure 12(a–f) illustrated the FESEM images of anodic TiO_2 nanotube arrays obtained after anodization of Ti-6Al-7Nb for 1 h at 30 V in an electrolyte consisting of 1 M H_2SO_4 and 0.08 M HF at 5, 10, 25, 30, 50 and 70 °C. The sample anodized at 5 °C (Fig. 12a) revealed a premature porous structure with an un-dissolved oxide layer on the surface. At 10 °C, a porous oxide layer with pore diameter ~35 nm covers the entire surface in an irregular pattern as shown in Fig. 12b. No clear wall separation and inter-tubular space noticed at this stage.

In Fig. 12c, TiO_2 nanotube arrays formation with an average inner pore diameter of 125 nm, length of ~250 nm, the wall thickness of 30 nm and an inter-tube space 35 nm were observed at 25 °C. Also, the morphology of the nanotubes was smooth and circular without any defect. FESEM images of samples anodized at 30, 50 and 70 °C (Fig. 12d–f) exhibited regular and vertically aligned tube structure.

The effect of decreased electrolyte temperature on anodization was also studied by Wang et al. [82]. It was reported that there is a decrease in nanotube diameter and increase in wall thickness on anodization done in glycerol-based aqueous electrolyte kept in an ice bath.

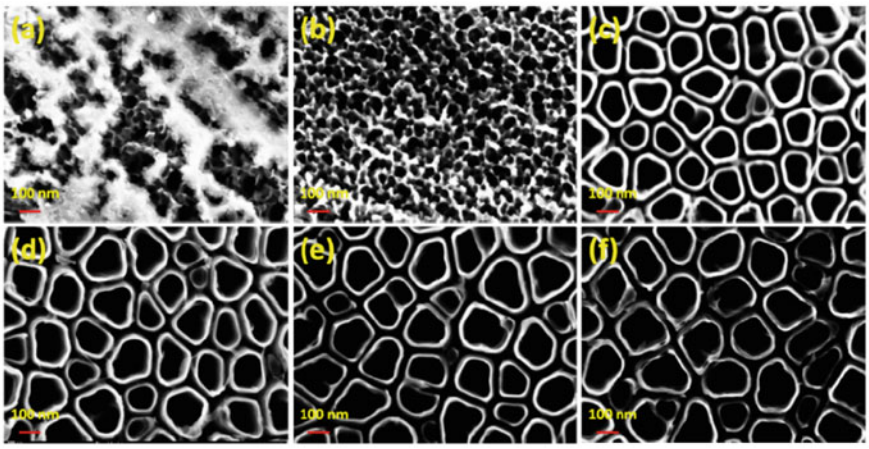

Fig. 12 FESEM images (top view) of samples anodized at different temperatures **a** 5 °C. **b** 10 °C. **c** 25 °C. **d** 30 °C. **e** 50 °C. **f** 70 °C (Reprinted with permission from [61])

7.5 Effect of Electrolyte pH

Acid, salt or alkaline solutions have been widely used as electrolytes for the anodization of titanium to achieve a varied range of oxide layer thickness [83]. The dissolubility of the electrolyte and the hydrolysis ability of the oxide layer are influenced by the p^H of the electrolyte [72]. The different p^H electrolyte has an impact on the chemical reaction rate of the etching of the porous oxide layer, which results in the formation of TiO_2 nanotubes. Previous reports clearly showed the formation of nanotubes by anodizing titanium substrate in 60 ml of 0.15 NH_4F at 20 V for 1 h at a pH ranges from 2 to 4 values. At this pH range, the tube length was found to increase with an increase in pH. While the anodization is done at low p^H, the high concentration of H^+ ions enhances the dissolution reaction of the oxide layer leading to shorter nanotube formation. Similarly, at high p^H as the concentration of H^+ ions decrease the dissolution rate of the oxide layer also decreases, leading to the increase in length of the nanotubes by increasing the anodization process [84, 85]. An increase in nanotube length from 1.2 μm to 6.0 μm for electrolyte p^H values of 3.0 and 5.0 respectively, after 17 h of anodization was reported [86]. For an acidic range pH (1–6), an increase in tube length from 3.5 to 5.3 μm under the same voltage and time conditions. In alkaline electrolyte, with pH 10 and pH 12, the length of nanotubes obtained was found to be 5.6 and 1.8 μm respectively [60].

8 Anodization of Titanium Alloys

Basically, titanium alloys are classified as α, near-α, α + β, metastable β, or stable β depending upon the room temperature microstructure [87]. In this aspect, titanium alloying elements can be classified as α-stabilizers (Al, O, N, C), β-stabilizers (Nb, V, Ta, Fe Cr, Si, Co, Mn) and neutral such as Zr [72]. Titanium alloys are widely used in hard tissue replacements in artificial bones, joints and dental prosthetic applications. Various attractive properties of the Ti-based alloys such as high corrosion resistance, exceptional mechanical properties and good biocompatibility were the driving force for the early introduction of α (Cp-Ti) and α + β (Ti–6Al–4 V, Ti-6Al-7Nb) alloys as well as the more recent development of modern and orthopaedic metastable β Ti and β stabilized Ti alloys [16, 27]. Several studies reported the formation of nanotubes on different Ti alloys [61, 88–94]. Nakada et al. [95] suggested using Ti-Nb-Ta-Zr (TNTZ) alloy for orthopaedic implants because of its exceptional mechanical properties, biocompatibility and anticorrosion properties. In another study, an anodized nanotube oxide layer with two size scale structures was reported on Ti-28Zr-8Nb alloy using buffered electrolyte [96]. The influence of alloy composition on the formed anodic oxide layer morphology on binary titanium alloys such as Ti-xTa, Ti-yZr, and Ti–Al was investigated by the researchers [89, 97]. The study revealed the formation of nanotube arrays on Ti-Zr alloy with a decreased diameter and increased tube length with increasing zirconium content. A tantalum oxide (Ta_2O_5) porous layer with pore diameter ranges from 2 to 35 nm on tantalum metal can be formed electrochemically in acid-containing HF as electrolyte [98]. Highly ordered Ta_2O_5 nanoporous layer have grown on tantalum foils by anodization using glycerol and NH_4F containing electrolyte and it was found that average pore diameter and thickness were affected by the NH_4H concentration [99].

Anodization of CP Ti and titanium alloys (Ti-6Al-4 V, Ti-6Al-7Nb, Ti-13Nb-13Zr, and β-21s) has investigated at optimized parameter [61]. FESEM images (left side at lower and right side at higher magnifications) of anodic TiO_2 nanotube arrays (TNT) obtained after anodization of CP Ti, Ti-6Al-4V, Ti-6Al-7Nb, Ti-13Nb-13Zr and β-21S for 1 h in an electrolyte consisting of 1 M H_2SO_4 and 0.08 M HF at 25 °C are shown in Fig. 13 (a–e). Highly ordered, regular and vertically aligned TNT structures were observed on CP Ti, Ti-6Al-4V and Ti-6Al-7Nb as shown in Fig. 13a–c. The metastable β alloy, Ti-13Nb-13Zr given in Fig. 13d showed the formation of nanostructured dual morphology with varied pore diameters. In the same image, a high degree of ordering in tubes was visible beneath the small porous structure. On the contrary, beta alloy, beta-21S in Fig. 13e showed no sign of nanotubular morphology due to composition of electrolyte solution used, whereas, the electrolyte with 0.25 M NH_4F in ethylene glycol reported the formation of nanotubular structure [98]. At higher magnification (right side), random structure was observed. Thus, at various compositions and at fixed parameters such as time (1 h), temperature (25 °C) and electrolyte composition, titanium alloys exhibit significant properties.

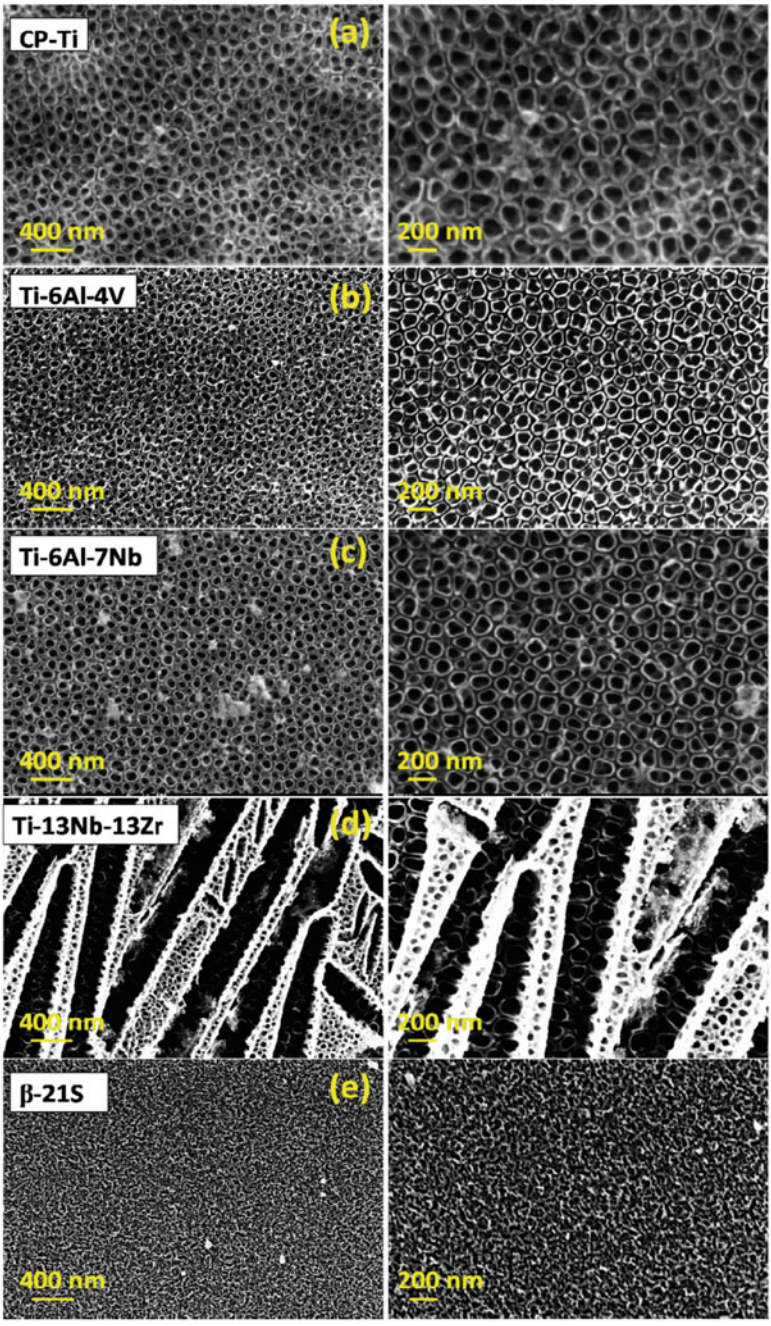

Fig. 13 FESEM images (top view) of different Ti samples anodized for 1 h at 25 °C. **a** CP Ti. **b** Ti-6Al-4 V. **c** Ti-6Al-7Nb. **d** Ti-13Nb-13Zr. **e** β-21s (Reprinted with permission from [61])

Due to the presence of the valve metals such as Al, Nb, Zr in the alloy composition, nanotubular structure with similar morphology were able to form on CP Ti with α phase, Ti-6Al-4V, and Ti-6Al-7Nb with α + β alloys.

9 Functionalization of Titania Nanotubular Structures

The TiO_2 nanostructures formed via electrochemical anodization process have been widely explored as a favorable biomaterial for a wide range of biomedical applications. Bone cell adhesion, growth and differentiation, prevention of bacterial adhesion, apatite forming abilities, drug delivery were demonstrated on nanostructured titania surfaces, showing its potential as bone implants [100–102]. For improved adhesion of cells on the nanostructures, it is essential to improve the surface functionalities of these nanostructures.

9.1 Surface Functionalization with Inorganic Bioactive Agents

The surface modification of titania nanotubes is necessary for improving the biocompatibility via introduction of new properties and functionalities. The tubular structure of titanium favours the incorporation of various inorganic bioactive agents to impart some specific properties. The bioactivity and antibacterial activity of nanotubes can be improved by the incorporation of antibiotics, growth factors, antibacterial agents, bone growth enhancement agents and anti-inflammatory agents. Loading of various inorganic bioactive elements such as silver, strontium, zirconium and zinc were demonstrated to achieve long term antibacterial activity and osteogenesis induction [103]. Nanotubes not only facilitate the loading of these agents, but also provide a means to control the loading capacity and release rate by varying the structural parameters.

To improve the benefits of TiO_2 nanotubes, we have incorporated various inorganic bioactive agents such as Strontium, Zirconium and Zinc ions into titania nanotubes and investigated its biocompatibility and electrochemical behaviour in stimulated body fluid environment. Indira et al. [104] reported the incorporation of Zr over TNT surface via dip coating method. The FE-SEM micrographs and the corresponding EDS spectra of TNT and Zr-TNT are shown in Fig. 14a–h. The nanotubes have an average pore diameter of 110 ± 4 nm and a wall thickness of 15 ± 2 nm respectively (Fig. 14a and b). The average inter pore diameter is about 128 ± 2 nm. Apparently, the layer consists of arrays of individual nanotubes with a length of 2.1 ± 0.3 μm (Fig. 14c). The presence of Ti, O and trace amount of F on the TNT surface was determined from the EDS spectrum.

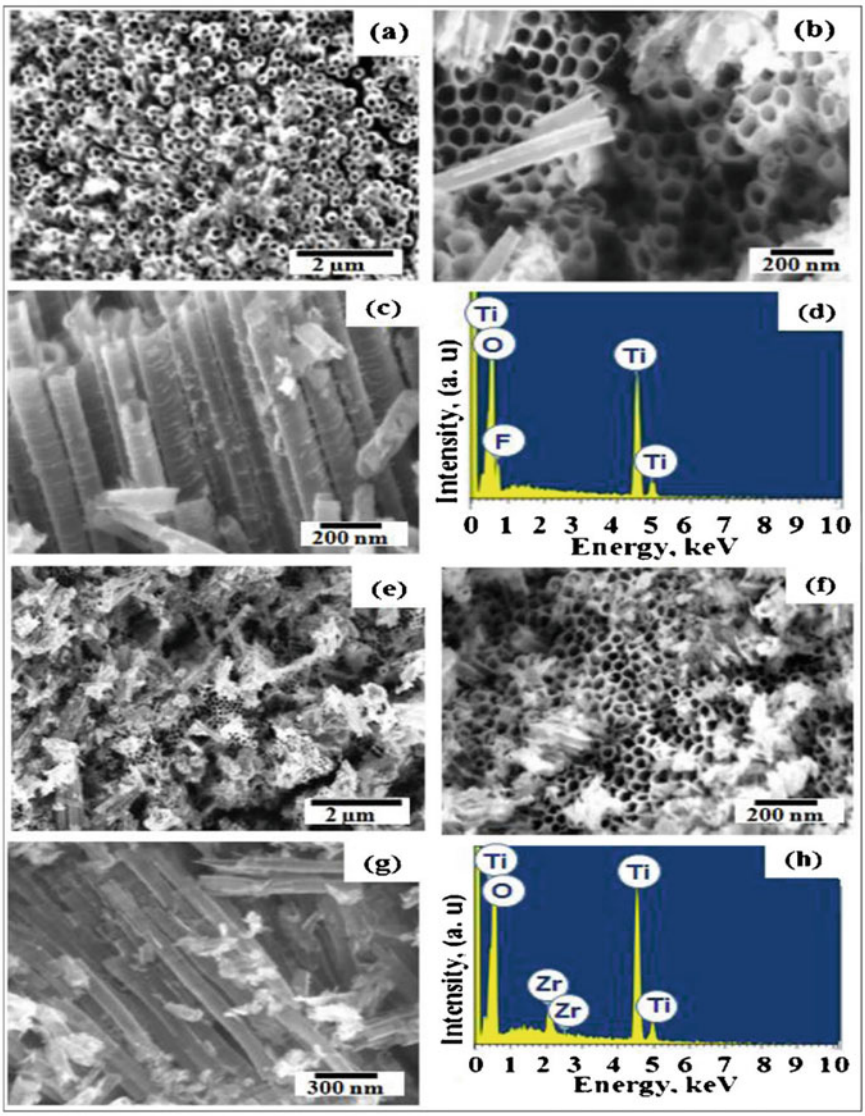

Fig. 14 **a–h** shows the FE-SEM micrographs and the corresponding EDS spectra of TNT and Zr-TNT (Reprinted with permission from [104])

Cluster like particles was observed over the TNT surface (Fig. 14e) after the treatment with $ZrOCl_2$ solution. The original tubular structure of TNT (Fig. 14f) was retained even after the incorporation of Zr ions, however, a small decrease (11 ± 5 nm) in the diameter was observed. The average pore diameter, wall thickness and tube length of Zr-TNT were found to be 99 ± 5 nm, 25 ± 3 nm and 2.3 ± 0.2 µm

respectively. The developed Zr-TNT is supposed to be a good implant material in bio environment with biocompatibility, improved corrosion resistance and is likely to be widening the biomedical application of titanium implants with new surface properties in the nanoscale regime.

Strontium ranelate, is widely used clinically for the treatment of osteoporosis due to the biological importance of strontium. Administration of a suitable dose of strontium can promote bone formation and inhibit bone resorption, leading to enhance bone mass [105]. Indira et al. [106] also reported the fabrication of Sr–TNTA on titanium substrate by a simple dip-coating method on anodic TNTA. The FE-SEM micrographs and EDS spectra of the specimens are shown in Fig. 15a–h. Nanotubes arrays (Fig. 15c) with an average diameter and wall thickness of 110 ± 4 nm and 15 ± 2 nm, respectively were observed after the anodization of titanium. After deposition, the walls of the tube were covered with Sr ions. Also, some clusters of Sr ions were scattered over the top of TNTA surface. The TNTA (Fig. 15g) retained the unique nanotubular morphology even after the incorporation of Sr ions, however, a small decrease in the diameter during the transformation of TNTA to Sr-TNTA, was noticed, which may probably due to volume expansion during the conversion of titanium oxide to strontium titanate.

Orthopaedic implant failure has been a major concern for orthopaedic surgeons over the past decades. Poor osseointegration together with bacterial infection is one of the major reasons for implant failure. Hence titanium implants having enhanced osseointegration and antibacterial property to prevent implant-associated infection are highly desirable for the long term success of implants. To address this problem, zinc incorporated titania nanotube arrays (Zn-TNTA) were developed on titanium surface to enhance the biocompatibility and also to ensure antibacterial properties [59, 107]. Here in this study the incorporation of Zn into TNTA was achieved by simple dip-coating method. Different concentrations of zinc solution (0.25, 0.5, 1.0 and 1.5 M $Zn(OH)_2$ solution) were prepared to study the nature of deposition of zinc into the nanotubes. The samples were designated as NT-Zn (0.25 M), NT-Zn(0.5 M), NT-Zn(1.0 M) and NT-Zn(1.5 M) respectively. Our observations reveal that uniform deposition of zinc into the nanotubes can be achieved by dip-coating method. The dipping and lifting of the TNTA specimens enable the zinc hydroxide solution to penetrate into and between the nanotubes and get uniformly deposited along the entire length of the nanotubes.

Figure 16a–d represents the HR-SEM images of NT-Zn (0.25 M), NT-Zn (0.5 M), NT-Zn (1.0 M) and NT-Zn (1.5 M) specimens. As apparent from the SEM images, NT-Zn (0.25 M), NT-Zn (0.5 M), NT-Zn (1.0 M) and NT-Zn (1.5 M) exhibit quite different morphologies. As can be seen in Fig. 16a, for NT-Zn (0.25) M specimen, the filling of zinc initiates at the pores and randomly deposited at the surface of the nanotubes. At 0.5 M (Fig. 16b), concentration, a homogenous distribution of zinc oxide at the tube walls and intertubular spaces were obtained. The nanotube structures were not masked due to the filling of zinc oxide. However, the diameter of the nanotubes decreases after the incorporation of zinc oxide. At 1.0 M concentration (Fig. 16c), ZnO deposited on the TNTA surface appeared in the form of flakes and started to mask the nanotubes. The formation of typical ZnO “nanoflowers” was

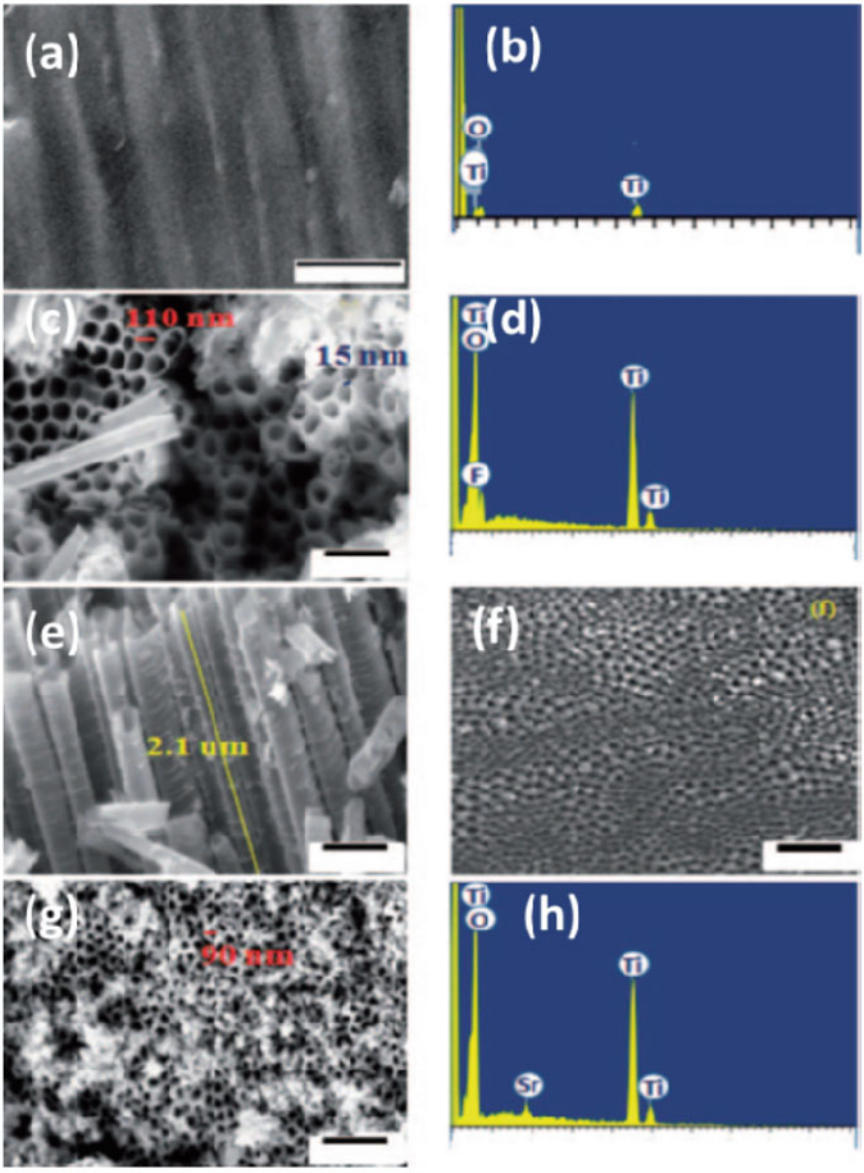

Fig. 15 FE-SEM images of (a) untreated Ti, (c) TNTA (e) cross sectional view of TNTA and (f) bottom view of TNTA and (g) Sr-TNTA and EDS spectrum of (b) untreated Ti, (d) TNTA and (h) Sr-TNTA (Reprinted with permission from [106])

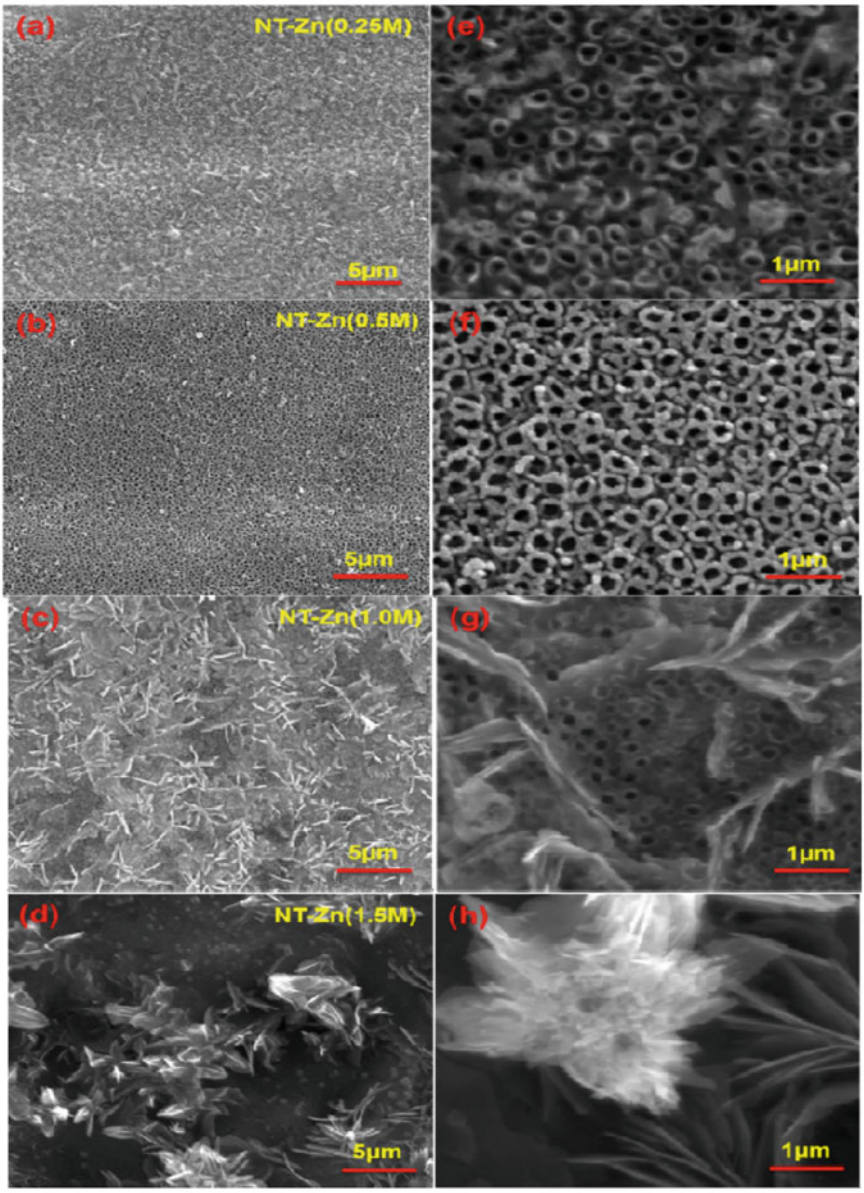

Fig. 16 HR-SEM images and corresponding higher magnification images of (a and e) NT-Zn (0.25 M), (b and f) NT-Zn (0.5 M), (c and g) NT-Zn (1.0 M) and (d and h) NT-Zn (1.5 M) specimens (Reprinted with permission from [59])

observed on the TNTA surface at 1.5 M concentration (Fig. 16d) and it fully covered the nanotube surface which was more clearly visualized in its corresponding higher magnification image provided in Fig. 16h.

Among the various concentrations studied, homogenous deposition of zinc oxide was observed at 0.5 M. Uniform deposition of zinc by retaining the tubular nature of the titania nanotubes is more advantageous for implant applications.

9.2 Surface Functionalization Using Polypyrrole

To tailor the surface properties of TiO_2 nanotubes and to advance their surface properties applicable to a wide variety of biomedical applications, an attempt has been made to synthesis Polypyrrole/Titania nanotube arrays (PPy-TNTA) hybrid on titanium surface [108]. PPy-TNTA hybrid was prepared by normal pulse voltammetry electrodeposition process in an electrolyte solution containing 0.2 M $LiClO_4$ and 0.1 M pyrrole. To benefit pyrrole monomer deposition, the pulse width was adjusted at 0.06 s and the pulse period was controlled at 4 s and 6 s respectively. The HR-SEM images for TNTA and PPy deposited on TNTA at various pulse potential 4 s and 6 s, and their corresponding cross-sectional images are demonstrated in Fig. 17a–f. The morphological differences became apparent, upon comparing the micrographs of the TNTA and the PPy-TNTA surface.

As evident from the images, at a pulse potential 4 s, the in-filtered PPy initially fills the Intertubular space between the nanotubes and then partially covered at the surface of the nanotubes. Further the pores of the TNTA were increasingly filled with

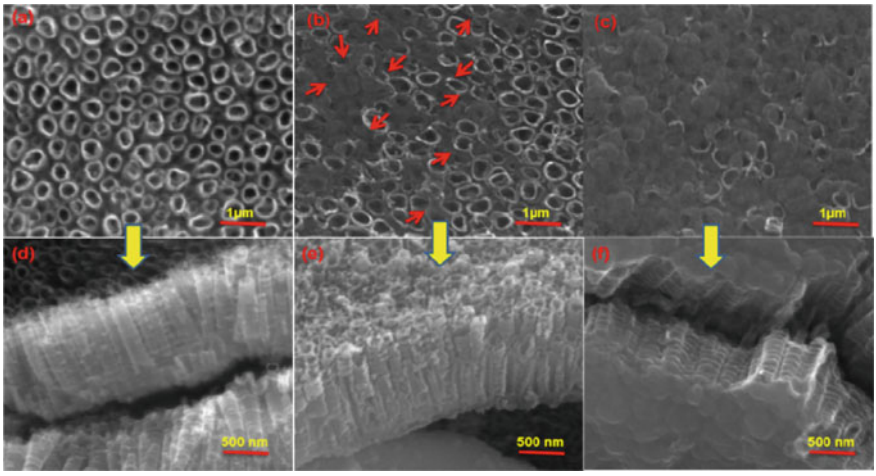

Fig. 17 HR-SEM images (a, b, c) and corresponding cross-sectional images (d, e, f) of TNTA, PPy -TNTA at 4 s and PPy-TNTA at 6 s (Reprinted with permission from [108])

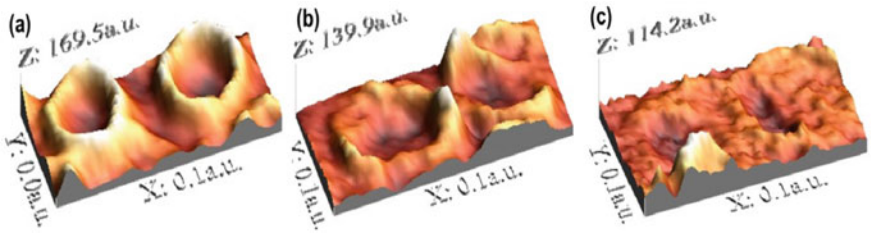

Fig. 18 3D images of a pair of **a** TNTA. **b** PPy/TNTA at pulse potential 4 s and **c** PPy-TNTA at pulse potential 6 s specimens (Reprinted with permission from [108])

PPy with an increase in pulse potential to 6 s. Moreover, a densely packed polymer film with spherical morphology was observed on the nanotube surface.

The 3D images obtained from HR-SEM images for a pair of nanotubes of TNTA and PPy-TNTA at pulse potential of 4 s and 6 s respectively are given in Fig. 18a–c. The deposition of polypyrrole initially into the spaces between the tubes, then inside the tubes, and if prolonged on the surface of the nanotubes can be achieved by electropolymerization under controlled pulse potential conditions.

The results of the above study indicated that the improved surface properties of PPy/TNTA pave the way towards the employment of the newly developed hybrid material as a viable substitute in biomedical field, especially in the field of orthopedic implants.

9.3 Surface Functionalization Using Plasma Nitriding

Now a days, pure titanium and $\alpha + \beta$ type Ti-6Al-4V alloys are commonly used as structural and/or functional biomaterials for replacement of hard tissues in devices such as artificial hip or knee replacements and dental implants [109]. The properties such as excellent corrosion resistance in the body fluid medium, no adverse tissue reactions, high mechanical strength, low modulus, low density and good wear resistance are expected to be possessed by an ideal biomaterial for implant applications. The tribological properties of titanium alloys can be enhanced using surface modification. It is possible to obtain surface layers consisting of titanium nitrides through physical and chemical vapour deposition, laser treatments, ion implantation and thermal nitriding [110]. The high hardness and low coefficient of friction of Titanium nitride (TiN) coatings allow the improvement of wear resistance of the substrate materials and hence widely used in many industrial coating technologies. The corrosion resistance properties of substrate material in many aggressive environments can be improved by TiN coatings [111]. The nitriding behaviour of pure titanium and its most popular alloy Ti-6Al-4V has been well documented [112–119] and the results of these studies show that effective nitriding takes place at temperatures close to the beta transus temperatures.

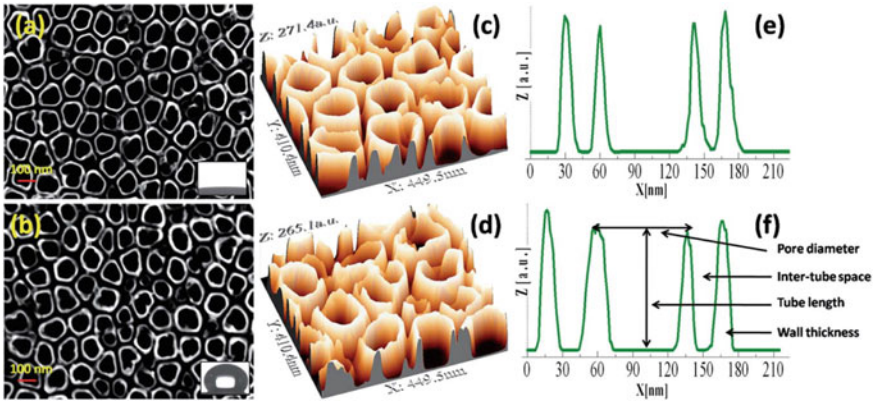

Fig. 19 FESEM images of TNT (a) and TNT + PN (b) (top view) inset water contact angle, (c) and (d) 3D images at higher magnification obtained from FESEM image and 2D profile of the nanotubes (e) and (f) (Republished with permission of the Royal Society of Chemistry, from Mohan et al. [120])

Mohan et al. [120] reported the effect of plasma nitriding on the structure and biocompatibility of self-organised TiO_2 nanotubes on Ti–6Al–7Nb alloy. Figure 19a shows the FESEM image of TNT obtained after anodisation of Ti-6Al-7Nb for 1 h at 20 V. The FESEM image of TNT plasma nitrided at 800 °C (TNT +PN) was shown in Fig. 19b. The 3D image of the TNT and TNT + PN obtained from FESEM image, respectively are given in Fig. 19c and d. The 3D images evidenced the formation of highly ordered tubes on Ti-6Al-7Nb. Similarly, Fig. 19e and f shows the 2D profile of the TNT and TNT + PN obtained respectively from FESEM images. FESEM images of the TNT and TNT + PN revealed that the arrays have very regular and vertically aligned tube structure. For TNT and TNT + PN samples, the nanotubes have diameters of approximately 100 and 80 nm and an average inter-tube distance of approximately 30 and 35 nm respectively as demonstrated in figure. The height of the TNT is approximately 250 nm. These results indicate that there is no much change in tubular dimensions after nitriding.

Nanohardness measurement was carried out on substrate, plasma nitrided substrate, TNT and TNT + PN samples at 0.5 mN load to study the effect of nitriding in improving the hardness of the specimens Five indentations were taken at different sites to check the uniformity of the coating hardness. Figure 20a and b shows the FESEM images of samples after NHT on TNT and TNT + PN samples respectively. The 3D image of the TiO_2 nano tube array generated from FESEM image for the same are shown in Fig. 20c and d. Similarly, Fig. 20e and f shows the 2D profile of the nano indentation on TiO_2 nanotube array obtained from FESEM images after NHT. After plasma nitriding, the hardness ofTi-6Al-7Nb has increased to 15.5 GPa than the substrate value of 9.2 GPa. Similarly, the hardness of the TNT and TNT + PN was 1.4 and 2.2 GPa, respectively. The nanoindentation studies showed that the mechanical properties of the TNT + PN are better than that of TNT. Nitriding

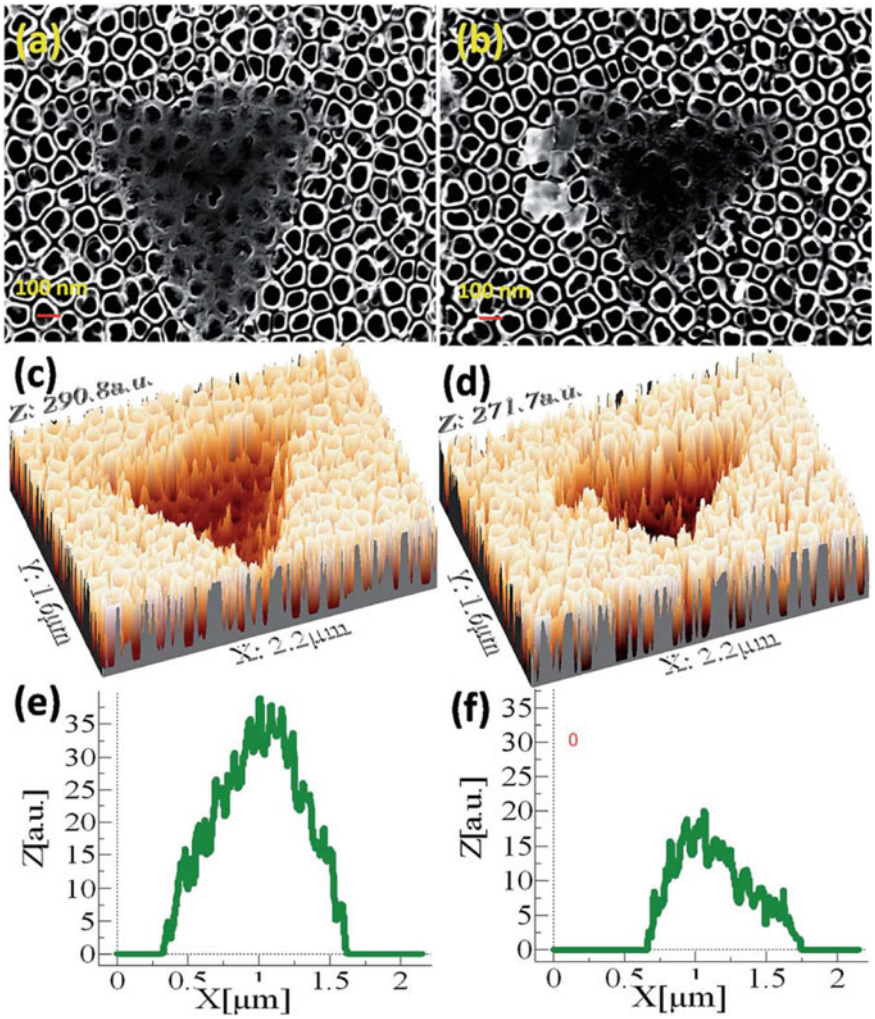

Fig. 20 FESEM images after NHT for TNT and TNT + PN samples. **a** and **b** 3D images obtained from FESEM image. **c**, **d**, **e** and **f** 2D profile of the nano indentation on TNT and TNT + PN (Republished with permission of the Royal Society of Chemistry, from Mohan et al. [120])

of nano tubes helps in increasing the hardness of the TiO_2 nanotubes that enhances formation of calcium phosphate phases.

9.4 Functionalization Using Tetrahedral Amorphous Carbon (Ta-C)

Diamond-like carbon (DLCs) with "higher sp^3 contents are termed as tetrahedral amorphous carbon (ta-C) and their hydrogenated analogue, ta-C:H [23, 121–127]. Tetrahedral amorphous carbon (ta-C) is extensively used as a coating material because of its properties such as high hardness, chemical inertness, superior wear resistance and low coefficient of friction comparable to diamond [128]. It has been demonstrated that the exceptional mechanical behavior of ta-C is mostly determined by its high percentage of sp^3 hybridization [129]. These properties make it ultimate for wear resistance on automotive components, cutting tools, aerospace components and biomedical applications. Mohan et al. [130] fabricated nanotubes on Ti–6Al–7Nb alloy by anodisation and filled tetrahedral amorphous carbon (ta-C) into nanotubes by cathodic arc evaporation method and characterized them for their nanoscale features".

FESEM image of an anodic TiO_2 nanotube array (TNT) obtained after anodisation of Ti–6Al–7Nb for 1 h at 30 V is shown in Fig. 21a. In this image, high degree of ordering of tubes can be seen. Figure 21b–f "shows the FESEM images of TNT filled with tetrahedral amorphous carbon (ta-C) for 0.5, 1, 2, 5 and 10 min, respectively. As can be seen from Fig. 21b, in 0.5 min, filling of ta-C takes place in inter-tubular space and pores. After 1 min, ta-C filled into inter-tubular space and pores formed network like growth of carbon can be seen from Fig. 21c. In Fig. 21d, 2 min filling, shows nodular like structure. Similarly, after 5 min in Fig. 21e, uniform spherical shape morphology can be seen which has covered the tubular pores and porous space. Further increase in deposition time to 10 min, the formed spherical morphology fuse together and completely covers the TNT which can be seen in Fig. 21f. From the figures, it can be seen that the gradual filling of the TNT by ta-C is taking place with increasing deposition time. The roughness values decrease due to an increase in the filling time resulting in a smoother layer. To demonstrate the filling rate of nanotubes 3D analyses was carried out on TNT and ta-C filled TNT samples. Figure 22a–f shows the 3D images obtained from FESEM images for single nanotube of TNT and ta-C filled TNT samples at 0.5, 1, 2, 5 and 10 min, respectively".

9.5 Loading of Quercetin and Chitosan into Nanotubes for Drug Delivery

Many researchers have investigated titanium nanotubes based drug-releasing implants (DRIs) in medical fields, such as "orthopedic implants, dental implants, vascular (coronary) stents, bone tissue engineering and localized cancer therapy" [33, 131, 132]. "Several therapeutic agents such as antibiotics, antifungal, anti-inflammatory, anticancer drugs, bone proteins, peptides, enzymes, vitamins, hormones, genes, antibodies, neurotransmitters, drug nanocarriers and nanoparticles have been applied in order to employ a wide range of therapies into titanium

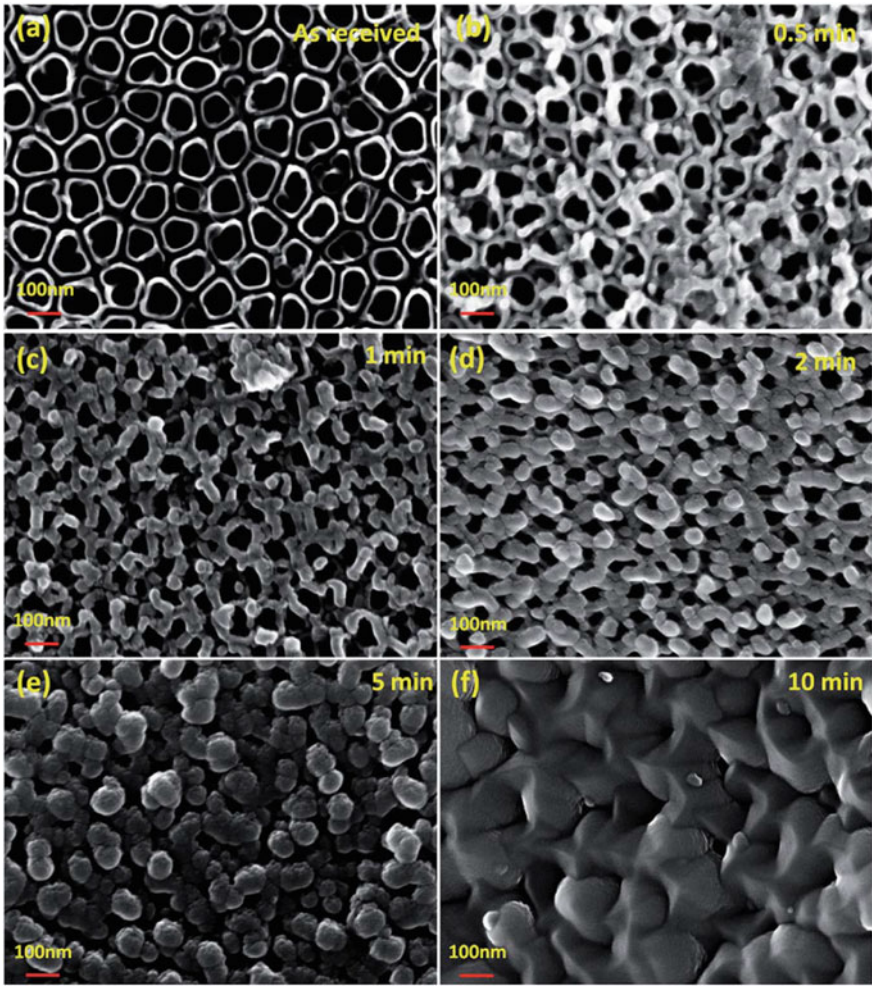

Fig. 21 FESEM images of TNT (a) and ta-C filled TNT samples at (b) 0.5 min, (c) 1 min, (d) 2 min, (e) 5 min and (f) 10 min (Republished with permission of the Royal Society of Chemistry, from Mohan et al. [130])

nanotubes based implants [132–134]. The critical parameters required for clinical applications such as desired kinetics, drug release rate and concentration for different localized drug delivery therapies are successfully delivered by titanium nanotubes as demonstrated by in vitro studies".

Local drug delivery develops into a prospective to conquer the drawbacks of conventional systemic administration by transporting out straight and local delivery of drugs from implants with nanopores/nanotubes. Local drug delivery systems

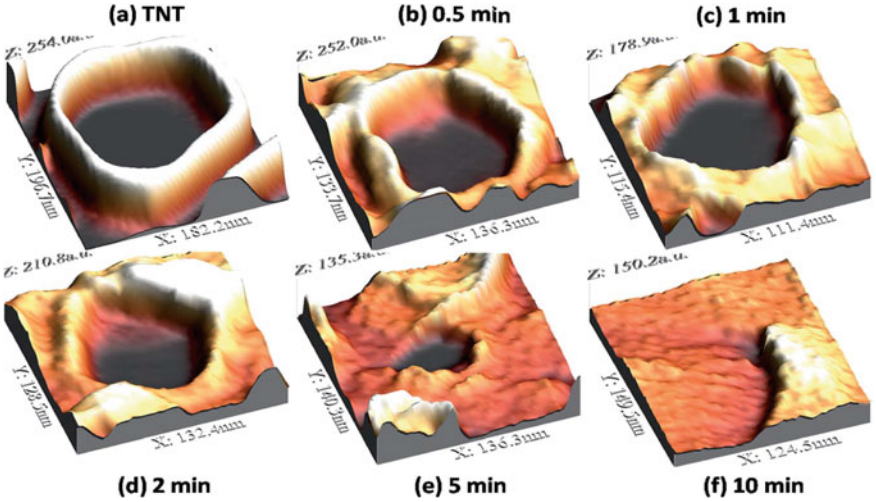

Fig. 22 3D images obtained from FESEM images for single nanotube (a) TNT and ta-C filled TNT samples at (b) 0.5 min, (c) 1 min, (d) 2 min, (e) 5 min and (f) 10 min (Republished with permission of the Royal Society of Chemistry, from Mohan et al. [130])

(drug-releasing implants) is capable of application in several areas, such as minimize the inflammatory reactions, bone infections treatment, progress and support of bone healing, osseointegration enhancement, and narrow treatment of bone cancers.

The TNT formed on Ti-6Al-7Nb (30 V) was filled with biopolymer chitosan [135]. 0.2 ml of chitosan was filled on the top of the quercetin filled nanotubes at various concentrations 0.5, 1 and 2% 0.10 mg of quercetin was dissolved in 0.2 ml of ethanol and incorporated into nanotubes by top filling method. FESEM images of the TNT filled with chitosan with different concentrations are shown in Fig. 23.

The filling of TNT with polymer was verified using 3D analysis. The 3D images of the polymer filled TNT obtained from the FESEM images are shown in Fig. 24. As can be seen from the figures the filling of chitosan has taken place gradually into the TNT. In case of 0.5%, filling of chitosan takes place in inter-tubular space and pores. In 1%, chitosan filled into inter-tubular space and pores formed regularly arranged pit like morphology. Similarly, in 2% chitosan filled TNT, uniform smooth morphology can be seen which has completely covered the tubular structure.

Figure 25 show the 3D images obtained from FESEM images for single nanotube of chitosan filled TNT samples at 0.5, 1 and 2%, respectively. Similarly, 2D profiles for the same are also given in the figure. After chitosan filling at various concentrations, the height and diameter of the nanotube decreases with a progressive filling of chitosan into TNT. The thickness of the chitosan filled at various concentrations was found to be 0.6, 1 and 3 μm for 0.5, 1 and 2% chitosan, respectively. Hence, thickness increased with an increase in chitosan concentration.

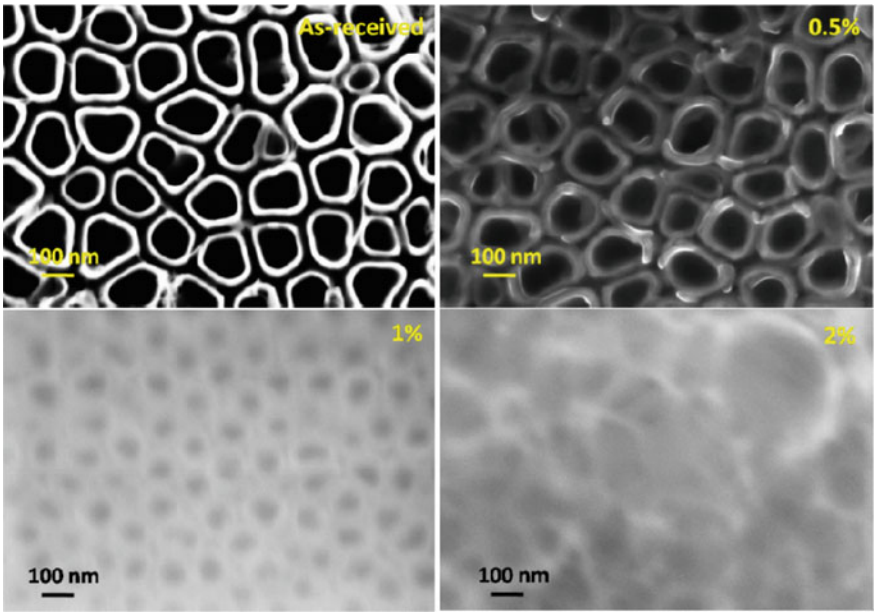

Fig. 23 FESEM images of TNT filled with bio-polymer (chitosan) at different concentrations (Reprinted with permission from [135])

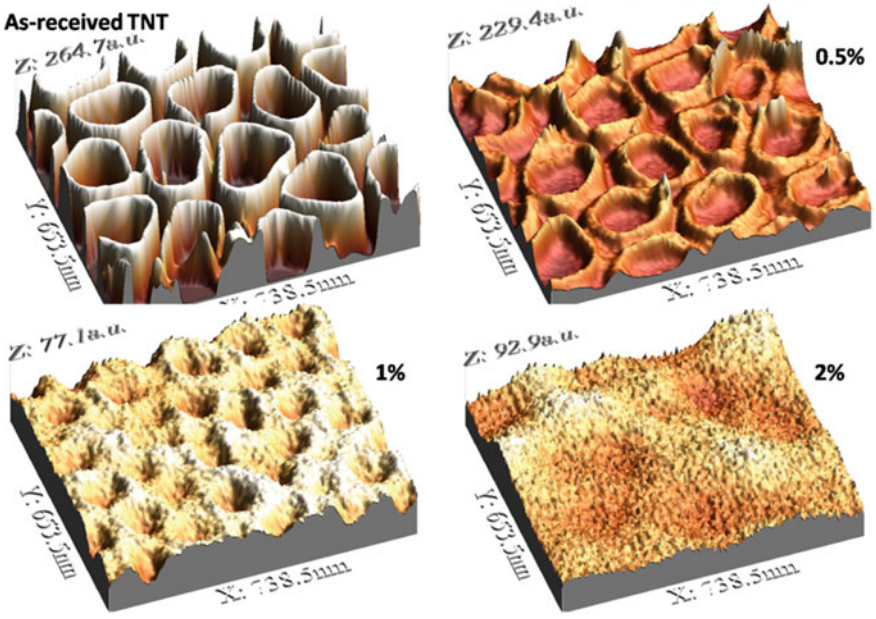

Fig. 24 3D images of polymer filled TNT obtained from FESEM images (Reprinted with permission from [135])

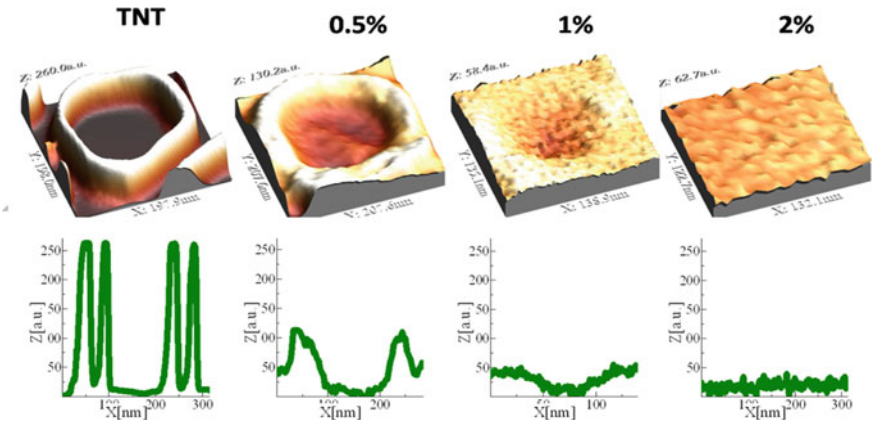

Fig. 25 3D and 2D profiles of polymer filled TNT obtained from FESEM images (Single nanotube) (Reprinted with permission from [135])

The authors also investigated the drug release from the drug-loaded nanotube samples by immersing in 30 ml of Hanks' solution. Drug release profiles of TNT loaded with quercetin are presented in Fig. 26 shows the overall releases.

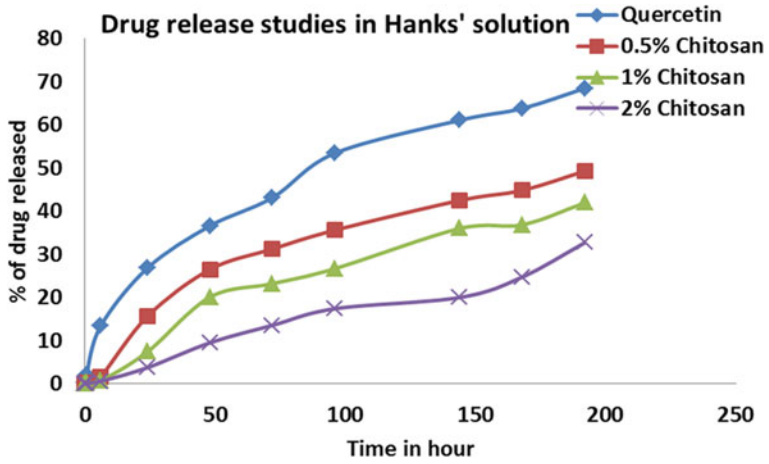

Fig. 26 Drug release graph of quercetin from TNT in Hanks' solution for 192 h (Reprinted with permission from [135])

10 Conclusions

Titania nanotube structures have received utmost attention in the medical domain due to its unique properties. An ordered nanotube with controllable morphology can be fabricated on titanium and its alloys by electrochemical anodization process. In this chapter, an overview of the formation of TiO_2 nanotubular structures on Cp-Ti, Ti-6Al-4 V, Ti-6Al-7Nb, Ti-13Nb-13Zr and β21S were discussed. The surface functionalization of nanotubes with the incorporation of various organic/inorganic bioactive agents such as polypyrrole, Zirconium, Strontium and Zinc were successfully implemented. The versatility of surface modification of Ti-6Al-7Nb via plasma nitriding for building new properties on titania nanotubes was demonstrated. The filling of nanotubes with ta-C using cathodic arc evaporation method is a promising surface modification to enhance the mechanical properties of titanium alloys. The drug and polymer loaded TNT can be used for the treatment of post-operative infection, inflammation and quick healing with better osseointegration. The various surface functionalities on nanotube surface discussed in this chapter have great potential to improve the properties of titanium and thus making it an attractive biomaterial and pave the way for the development of new biomedical devices with multiple functions.

References

1. Boretos JW, Eden M, Fung YC (1985) Contemporary biomaterials: material and host response, clinical applications, new technology and legal aspects. J Biomech Eng 107:87. https://doi.org/10.1115/1.3138526
2. Dennis C, Sethu S, Nayak S, Mohan L, Morsi Y, Manivasagam G (2016) Suture materials—current and emerging trends. J Biomed Mater Res—Part A 104:1544–1559. https://doi.org/10.1002/jbm.a.35683
3. Holzapfel BM, Reichert JC, Schantz JT, Gbureck U, Rackwitz L, Nöth U, Jakob F, Rudert M, Groll J, Hutmacher DW (2013) How smart do biomaterials need to be? A translational science and clinical point of view. Adv Drug Deliv Rev 65:581–603
4. Manivasagam G, Dhinasekaran D, Rajamanickam A (2010) Biomedical Implants: Corrosion and its Prevention—A Review ~!2009-12-22~2010-01-20~!2010-05-25~! Recent Patents Corros Sci 2:40–54. https://doi.org/10.2174/1877610801002010040
5. S. T, K. T, Patel P, G. F, K. T (2012) Diamond, diamond-like carbon (DLC) and diamond-like nanocomposite (DLN) thin films for MEMS applications. In: Microelectromechanical systems and devices. InTech
6. Santra TS, Liu CH, Bhattacharyya TK, Patel P, Barik TK (2010) Characterization of diamond-like nanocomposite thin films grown by plasma enhanced chemical vapor deposition. J Appl Phys 107:124320. https://doi.org/10.1063/1.3415548
7. Santra TS, Bhattacharyya TK, Tseng FG, Barik TK (2012) Influence of flow rate on different properties of diamond-like nanocomposite thin films grown by PECVD. AIP Adv 2:022132. https://doi.org/10.1063/1.4721654
8. Santra TS, Bhattacharyya TK, Mishra P, Tseng FG, Barik TK (2012) Biomedical applications of diamond-like nanocomposite thin films. Sci Adv Mater 4:110–113. https://doi.org/10.1166/sam.2012.1258

9. Santra TS, Bhattacharyya TK, Patel P, Tseng FG, Barik TK (2011) Structural and tribological properties of diamond-like nanocomposite thin films. Surf Coatings Technol 206:228–233. https://doi.org/10.1016/j.surfcoat.2011.06.057
10. Mechanical testing of orthopaedic implants, 1st edn. https://www.elsevier.com/books/mechanical-testing-of-orthopaedic-implants/friis/978-0-08-100286-5. Accessed 22 Jun 2020
11. McGregor DB, Baan RA, Partensky C, Rice JM, Wilbourn JD (2000) Evaluation of the carcinogenic risks to humans associated with surgical implants and other foreign bodies—a report of an IARC Monographs Programme Meeting. In: European J Cancer Eur J Cancer, pp 307–313
12. Chen Q, Thouas GA (2015) Metallic implant biomaterials. Mater. Sci. Eng. R Reports 87:1–57
13. Hu X, Shen H, Shuai K, Zhang E, Bai Y, Cheng Y, Xiong X, Wang S, Fang J, Wei S (2011) Surface bioactivity modification of titanium by CO_2 plasma treatment and induction of hydroxyapatite: In vitro and in vivo studies. Appl Surf Sci 257:1813–1823. https://doi.org/10.1016/j.apsusc.2010.08.082
14. Mohan L, Durgalakshmi D, Geetha M, Narayanan TSNS, Asokamani R (2012) Electrophoretic deposition of nanocomposite (HAp + TiO_2) on titanium alloy for biomedical applications. Ceram Int 38:3435–3443
15. Gittens RA, Olivares-Navarrete R, Schwartz Z, Boyan BD (2014) Implant osseointegration and the role of microroughness and nanostructures: Lessons for spine implants. Acta Biomater 10:3363–3371
16. Geetha M, Singh AK, Asokamani R, Gogia AK (2009) Ti based biomaterials, the ultimate choice for orthopaedic implants—a review. Prog Mater Sci 54:397–425. https://doi.org/10.1016/j.pmatsci.2008.06.004
17. Puleo DA, Nanci A (1999) Understanding and controlling the bone-implant interface. Biomaterials 20:2311–2321. https://doi.org/10.1016/S0142-9612(99)00160-X
18. Bajgai MP, Parajuli DC, Park SJ, Chu KH, Kang HS, Kim HY (2010) In vitro bioactivity of sol-gel-derived hydroxyapatite particulate nanofiber modified titanium. J Mater Sci Mater Med 21:685–694. https://doi.org/10.1007/s10856-009-3902-2
19. Mohan L, Anandan C, Rajendran N (2015) Electrochemical behavior and effect of heat treatment on morphology, crystalline structure of self-organized TiO_2 nanotube arrays on Ti–6Al–7Nb for biomedical applications. Mater Sci Eng, C 50:394–401. https://doi.org/10.1016/j.msec.2015.02.013
20. Gittens RA, McLachlan T, Olivares-Navarrete R, Cai Y, Berner S, Tannenbaum R, Schwartz Z, Sandhage KH, Boyan BD (2011) The effects of combined micron-/submicron-scale surface roughness and nanoscale features on cell proliferation and differentiation. Biomaterials 32:3395–3403. https://doi.org/10.1016/j.biomaterials.2011.01.029
21. Hang R, Zhao F, Yao X, Tang B, Chu PK (2020) Self-assembled anodization of NiTi alloys for biomedical applications. Appl. Surf, Sci, p 517
22. Monetta T, Acquesta A, Carangelo A, Bellucci F (2017) TiO_2 nanotubes on Ti dental implant. Part 1: Formation and aging in Hank's solution. Metals (Basel) 7:167. https://doi.org/10.3390/met7050167
23. Anandan C, Mohan L, Babu PD (2014) Electrochemical studies and growth of apatite on molybdenum doped DLC coatings on titanium alloy β-21S. Appl Surf Sci 296:86–94. https://doi.org/10.1016/j.apsusc.2014.01.049
24. Yang B, Uchida M, Kim H, Zhang X (2004) Preparation of bioactive titanium metal via anodic oxidation treatment. Biomaterials 25:1003–1010. https://doi.org/10.1016/S0142-9612(03)00626-4
25. Anandan C, Mohan L (2013) In vitro corrosion behavior and apatite growth of oxygen plasma ion implanted titanium alloy β-21S. J Mater Eng Perform 22:3507–3516. https://doi.org/10.1007/s11665-013-0628-6
26. Viswanathan S, Mohan L, Bera P, Kumar VP, Barshilia HC, Anandan C (2017) Corrosion and wear behaviors of cr-doped diamond-like carbon coatings. J Mater Eng Perform 26:3633–3647. https://doi.org/10.1007/s11665-017-2783-7

27. Liu X, Chu PK, Ding C (2004) Surface modification of titanium, titanium alloys, and related materials for biomedical applications. Mater Sci Eng R Reports 47:49–121
28. Mohan L, Anandan C (2013) Wear and corrosion behavior of oxygen implanted biomedical titanium alloy Ti-13Nb-13Zr. Appl Surf Sci 282:281–290. https://doi.org/10.1016/j.apsusc.2013.05.120
29. Mohan L, Chakraborty M, Viswanathan S, Mandal C, Bera P, Aruna ST, Anandan C (2017) Corrosion, wear, and cell culture studies of oxygen ion implanted Ni–Ti alloy. Surf Interface Anal 49:828–836. https://doi.org/10.1002/sia.6229
30. Gnanavel S, Ponnusamy S, Mohan L, Muthamizhchelvan C (2018) In vitro corrosion behaviour of Ti–6Al–4 V and 316L stainless steel alloys for biomedical implant applications. J Bio-Tribo-Corrosion 4:1. https://doi.org/10.1007/s40735-017-0118-8
31. Gnanavel S, Ponnusamy S, Mohan L (2018) Biocompatible response of hydroxyapatite coated on near-β titanium alloys by E-beam evaporation method. Biocatal Agric Biotechnol 15:364–369
32. Anne Pauline S, Kamachi Mudali U, Rajendran N (2013) Fabrication of nanoporous Sr incorporated TiO_2 coating on 316L SS: evaluation of bioactivity and corrosion protection. Mater Chem Phys 142:27–36. https://doi.org/10.1016/j.matchemphys.2013.06.026
33. Bauer S, Schmuki P, von der Mark K, Park J (2013) Engineering biocompatible implant surfaces: Part I: Materials and surfaces. Prog Mater Sci 58:261–326
34. Mohan L, Kar S, Nandhini B, Dhilip Kumar SS, Nagai M, Santra TS (2020) Formation of nanostructures on magnesium alloy by anodization for potential biomedical applications. Mater Today Commun 25:101403. https://doi.org/10.1016/j.mtcomm.2020.101403
35. Lee K, Mazare A, Schmuki P (2014) One-dimensional titanium dioxide nanomaterials: nanotubes. Chem Rev 114:9385–9454
36. Tan aW, Pingguan-Murphy B, Ahmad R, Akbar Sa (2012) Review of titania nanotubes: fabrication and cellular response. Ceram Int 38:4421–4435. https://doi.org/10.1016/j.ceramint.2012.03.002
37. Mohan L, Anandan C, Rajendran N (2015) Electrochemical behaviour and bioactivity of self-organized TiO_2 nanotube arrays on Ti-6Al-4 V in Hanks' solution for biomedical applications. Electrochim Acta 155:411–420. https://doi.org/10.1016/j.electacta.2014.12.032
38. Simchi A, Tamjid E, Pishbin F, Boccaccini AR (2011) Recent progress in inorganic and composite coatings with bactericidal capability for orthopaedic applications. Nanomedicine Nanotechnology. Biol. Med. 7:22–39
39. Divya Rani VV, Vinoth-Kumar L, Anitha VC, Manzoor K, Deepthy M, Shantikumar VN (2012) Osteointegration of titanium implant is sensitive to specific nanostructure morphology. Acta Biomater 8:1976–1989. https://doi.org/10.1016/j.actbio.2012.01.021
40. Na SI, Kim SS, Hong WK, Park JW, Jo J, Nah YC, Lee T, Kim DY (2008) Fabrication of TiO_2 nanotubes by using electrodeposited ZnO nanorod template and their application to hybrid solar cells. Electrochim Acta 53:2560–2566. https://doi.org/10.1016/j.electacta.2007.10.041
41. Bae C, Yoo H, Kim S, Lee K, Kim J, Sung MM, Shin H (2008) Template-directed synthesis of oxide nanotubes: fabrication, characterization, and applications. Chem Mater 20:756–767. https://doi.org/10.1021/cm702138c
42. Yuan ZY, Su BL (2004) Titanium oxide nanotubes, nanofibers and nanowires. In: Colloids and surfaces a: physicochemical and engineering aspects. Elsevier, pp 173–183
43. Li G, Liu Z, Zhang Z, Yan X (2009) Preparation of titania nanotube arrays by the hydrothermal method. Cuihua Xuebao/Chinese J Catal 30:37–42. https://doi.org/10.1016/s1872-2067(08)60088-1
44. Song H, Qiu X, Li F, Zhu W, Chen L (2007) Ethanol electro-oxidation on catalysts with TiO_2 coated carbon nanotubes as support. Electrochem Commun 9:1416–1421. https://doi.org/10.1016/j.elecom.2007.01.048
45. Macak JM, Schmidt-Stein F, Schmuki P (2007) Efficient oxygen reduction on layers of ordered TiO_2 nanotubes loaded with Au nanoparticles. Electrochem Commun 9:1783–1787. https://doi.org/10.1016/j.elecom.2007.04.002

46. Tsuchiya H, MacAk JM, Ghicov A, Taveira L, Schmuki P (2005) Self-organized porous TiO_2 and ZrO_2 produced by anodization. Corros Sci 47:3324–3335. https://doi.org/10.1016/j.corsci.2005.05.041
47. Berger S, Faltenbacher J, Bauer S, Schmuki P (2008) Enhanced self-ordering of anodic ZrO2 nanotubes in inorganic and organic electrolytes using two-step anodization. Phys Status Solidi—Rapid Res Lett 2:102–104. https://doi.org/10.1002/pssr.200802019
48. Cipriano AF, Miller C, Liu H (2014) Anodic growth and biomedical applications of TiO_2 nanotubes. J Biomed Nanotechnol 10:2977–3003. https://doi.org/10.1166/jbn.2014.1927
49. Anitha VC, Menon D, Nair SV, Prasanth R (2010) Electrochemical tuning of titania nanotube morphology in inhibitor electrolytes. Electrochim Acta 55:3703–3713. https://doi.org/10.1016/j.electacta.2009.12.096
50. Fu Y, Mo A (2018) A review on the electrochemically self-organized titania nanotube arrays: synthesis, modifications, and biomedical applications. Nanoscale Re Lett 13
51. Macak JM, Tsuchiya H, Ghicov A, Yasuda K, Hahn R, Bauer S, Schmuki P (2007) TiO_2 nanotubes: self-organized electrochemical formation, properties and applications. Curr Opin Solid State Mater Sci 11:3–18
52. Gong D, Grimes CA, Varghese OK, Hu W, Singh RS, Chen Z, Dickey EC (2001) Titanium oxide nanotube arrays prepared by anodic oxidation. J Mater Res 16:3331–3334. https://doi.org/10.1557/JMR.2001.0457
53. Regonini D, Bowen CR, Jaroenworaluck A, Stevens R (2013) A review of growth mechanism, structure and crystallinity of anodized TiO_2 nanotubes. Mater Sci Eng R Reports 74:377–406
54. Valota A, Curioni M, Leclere DJ, Skeldon P, Falaras P, Thompson GE (2010) Influence of applied potential on titanium oxide nanotube growth. J Electrochem Soc 157:K243. https://doi.org/10.1149/1.3494155
55. Ali Yahia SA, Hamadou L, Kadri A, Benbrahim N, Sutter EMM (2012) Effect of anodizing potential on the formation and EIS characteristics of TiO_2 nanotube arrays. J Electrochem Soc 159:K83–K92. https://doi.org/10.1149/2.077204jes
56. Cai Q, Paulose M, Varghese OK, Grimes CA (2005) The effect of electrolyte composition on the fabrication of self-organized titanium oxide nanotube arrays by anodic oxidation. J Mater Res 20:230–236. https://doi.org/10.1557/JMR.2005.0020
57. Anodization parameters influencing the growth of titania nanotubes and their photoelectrochemical response. https://www.hindawi.com/journals/ijp/2012/638017/. Accessed 22 Jun 2020
58. Sulka GD, Kapusta-Kołodziej J, Brzózka A, Jaskuła M (2010) Fabrication of nanoporous TiO_2 by electrochemical anodization. Electrochim Acta 55:4359–4367. https://doi.org/10.1016/j.electacta.2009.12.053
59. Simi VS (2018) Fabrication of bioactive nanostructured titania for biomedical applications. Anna University, Chennai
60. Khudhair D, Bhatti A, Li Y, Hamedani HA, Garmestani H, Hodgson P, Nahavandi S (2016) Anodization parameters influencing the morphology and electrical properties of TiO_2 nanotubes for living cell interfacing and investigations. Mater Sci Eng, C 59:1125–1142
61. Mohan L, Dennis C, Padmapriya N, Anandan C, Rajendran N (2020) Effect of electrolyte temperature and anodization time on formation of TiO_2 nanotubes for biomedical applications. Mater Today Commun 101103. https://doi.org/10.1016/j.mtcomm.2020.101103
62. MacAk JM, Sirotna K, Schmuki P (2005) Self-organized porous titanium oxide prepared in Na_2SO_4/NaF electrolytes. Electrochim Acta 50:3679–3684. https://doi.org/10.1016/j.electacta.2005.01.014
63. Macak JM, Taveira LV, Tsuchiya H, Sirotna K, Macak J, Schmuki P (2006) Influence of different fluoride containing electrolytes on the formation of self-organized titania nanotubes by Ti anodization. J Electroceramics 16:29–34. https://doi.org/10.1007/s10832-006-3904-0
64. Paulose M, Prakasam HE, Varghese OK, Peng L, Popat KC, Mor GK, Desai TA, Grimes CA (2007) TiO_2 nanotube arrays of 1000 μm length by anodization of titanium foil: Phenol red diffusion. J Phys Chem C 111:14992–14997. https://doi.org/10.1021/jp075258r

65. Aw MS, Gulati K, Losic D (2011) Controlling Drug Release from Titania Nanotube Arrays Using Polymer Nanocarriers and Biopolymer Coating. J Biomater Nanobiotechnol 02:477–484. https://doi.org/10.4236/jbnb.2011.225058
66. Tsuchiya H, Macak JM, Müller L, Kunze J, Müller F, Greil P, Virtanen S, Schmuki P (2006) Hydroxyapatite growth on anodic TiO_2 nanotubes. J Biomed Mater Res—Part A 77:534–541. https://doi.org/10.1002/jbm.a.30677
67. Wan J, Yan X, Ding J, Wang M, Hu K (2009) Self-organized highly ordered TiO_2 nanotubes in organic aqueous system. Mater Charact 60:1534–1540. https://doi.org/10.1016/j.matchar.2009.09.002
68. Vasilev K, Poh Z, Kant K, Chan J, Michelmore A, Losic D (2010) Tailoring the surface functionalities of titania nanotube arrays. Biomaterials 31:532–540. https://doi.org/10.1016/j.biomaterials.2009.09.074
69. Simi VS, Rajendran N (2017) Influence of tunable diameter on the electrochemical behavior and antibacterial activity of titania nanotube arrays for biomedical applications. Mater Charact 129:67–79. https://doi.org/10.1016/j.matchar.2017.04.019
70. Macak JM, Hildebrand H, Marten-Jahns U, Schmuki P (2008) Mechanistic aspects and growth of large diameter self-organized TiO_2 nanotubes. J Electroanal Chem 621:254–266. https://doi.org/10.1016/j.jelechem.2008.01.005
71. Kaczmarek A, Klekiel T, Krasicka-Cydzik E (2010) Fluoride concentration effect on the anodic growth of self-aligned oxide nanotube array on Ti6Al7Nb alloy. Surf Interface Anal 42:510–514. https://doi.org/10.1002/sia.3303
72. Minagar S, Berndt CC, Wang J, Ivanova E, Wen C (2012) A review of the application of anodization for the fabrication of nanotubes on metal implant surfaces. Acta Biomater 8:2875–2888
73. Mîndroiu M, Pirvu C, Ion R, Demetrescu I (2010) Comparing performance of nanoarchitectures fabricated by Ti6Al7Nb anodizing in two kinds of electrolytes. Electrochim Acta 56:193–202. https://doi.org/10.1016/j.electacta.2010.08.100
74. Macak JM, Schmuki P (2006) Anodic growth of self-organized anodic TiO_2 nanotubes in viscous electrolytes. Electrochim Acta 52:1258–1264. https://doi.org/10.1016/j.electacta.2006.07.021
75. Raja KS, Gandhi T, Misra M (2007) Effect of water content of ethylene glycol as electrolyte for synthesis of ordered titania nanotubes. Electrochem Commun 9:1069–1076. https://doi.org/10.1016/j.elecom.2006.12.024
76. Mohamed AER, Kasemphaibulsuk N, Rohani S, Barghi S (2010) Fabrication of Titania nanotube arrays in viscous electrolytes. J Nanosci Nanotechnol 10:1998–2008. https://doi.org/10.1166/jnn.2010.2102
77. Von Der Mark K, Park J, Bauer S, Schmuki P (2010) Nanoscale engineering of biomimetic surfaces: Cues from the extracellular matrix. Cell Tissue Res 339:131–153
78. Lv L, Liu Y, Zhang P, Zhang X, Liu J, Chen T, Su P, Li H, Zhou Y (2015) The nanoscale geometry of TiO_2 nanotubes influences the osteogenic differentiation of human adipose-derived stem cells by modulating H3K4 trimethylation. Biomaterials 39:193–205. https://doi.org/10.1016/j.biomaterials.2014.11.002
79. Brammer KS, Frandsen CJ, Jin S (2012) TiO_2 nanotubes for bone regeneration. Trends Biotechnol 30:315–322. https://doi.org/10.1016/j.tibtech.2012.02.005
80. Mohan L (2016) Development of nanostructured titanium alloys for biomedical applications. Anna University, Chennai, India
81. Prida VM, Manova E, Vega V, Hernandez-Velez M, Aranda P, Pirota KR, Vázquez M, Ruiz-Hitzky E (2007) Temperature influence on the anodic growth of self-aligned Titanium dioxide nanotube arrays. J Magn Magn Mater 316:110–113. https://doi.org/10.1016/j.jmmm.2007.02.021
82. Jun W, Zhiqun L (2009) Anodic formation of ordered TiO_2 nanotube arrays: Effects of electrolyte temperature and anodization potential. J Phys Chem C 113:4026–4030. https://doi.org/10.1021/jp811201x

83. Fast-rate formation of TiO_2 nanotube arrays in an organic bath and their applications in photocatalysis—PubMed. https://pubmed.ncbi.nlm.nih.gov/20705970/. Accessed 22 Jun 2020
84. Chin LY, Zainal Z, Hussein MZ, Tee TW (2011) Fabrication of highly ordered TiO_2 nanotubes from fluoride containing aqueous electrolyte by anodic oxidation and their photoelectrochemical response. J Nanosci Nanotechnol 11:4900–4909. https://doi.org/10.1166/jnn.2011.4108
85. Sreekantan S, Lockman Z, Hazan R, Tasbihi M, Tong LK, Mohamed AR (2009) Influence of electrolyte pH on TiO_2 nanotube formation by Ti anodization. J Alloys Compd 485:478–483. https://doi.org/10.1016/j.jallcom.2009.05.152
86. Paulose M, Mor GK, Varghese OK, Shankar K, Grimes CA (2006) Visible light photoelectrochemical and water-photoelectrolysis properties of titania nanotube arrays. J Photochem Photobiol A Chem 178:8–15. https://doi.org/10.1016/j.jphotochem.2005.06.013
87. Oshida Y (2010) Bioscience and bioengineering of titanium materials. Elsevier
88. Jang SH, Choe HC, Ko YM, Brantley WA (2009) Electrochemical characteristics of nanotubes formed on Ti–Nb alloys. Thin Solid Films 517:5038–5043. https://doi.org/10.1016/j.tsf.2009.03.166
89. Tsuchiya H, Akaki T, Nakata J, Terada D, Tsuji N, Koizumi Y, Minamino Y, Schmuki P, Fujimoto S (2009) Anodic oxide nanotube layers on Ti-Ta alloys: Substrate composition, microstructure and self-organization on two-size scales. Corros Sci 51:1528–1533. https://doi.org/10.1016/j.corsci.2008.11.011
90. Xu R, Zhao J, Tao J, Wang X, Li Y (2008) Fabrication of Ti-Al-Zr alloy oxide nanotube arrays in organic electrolytes by anodization. J Appl Electrochem 38:1229–1232. https://doi.org/10.1007/s10800-008-9543-1
91. Yasuda K, Schmuki P (2007) Control of morphology and composition of self-organized zirconium titanate nanotubes formed in (NH4)2SO4/NH4F electrolytes. Electrochim Acta 52:4053–4061. https://doi.org/10.1016/j.electacta.2006.11.023
92. Tsuchiya H, Macak JM, Ghicov A, Tang YC, Fujimoto S, Niinomi M, Noda T, Schmuki P (2006) Nanotube oxide coating on Ti-29Nb-13Ta-4.6Zr alloy prepared by self-organizing anodization. Electrochim Acta 52:94–101. https://doi.org/10.1016/j.electacta.2006.03.087
93. Viswanathan S, Mohan L, Bera P, Anandan C (2016) Effect of oxygen plasma immersion ion implantation on the formation of nanostructures over Ni–Ti alloy. RSC Adv 6:74493–74499. https://doi.org/10.1039/C6RA11541A
94. Viswanathan S, Mohan L, John S, Bera P, Anandan C (2017) Effect of surface finishing on the formation of nanostructure and corrosion behavior of Ni–Ti alloy. Surf Interface Anal 49:450–456. https://doi.org/10.1002/sia.6178
95. Nakada H, Numata Y, Sakae T, Okazaki Y, Tanimoto Y, Tamaki H, Katou T, Ookubo A, Kobayashi K, LeGeros RZ (2008) Comparison of bone mineral density and area of newly formed bone around Ti-15%Zr-4%Nb-4%Ta alloy and Ti-6%A1-4%V alloy implants. J Hard Tissue Biol 17:99–108. https://doi.org/10.2485/jhtb.17.99
96. Feng XJ, Macak JM, Albu SP, Schmuki P (2008) Electrochemical formation of self-organized anodic nanotube coating on Ti–28Zr–8Nb biomedical alloy surface. Acta Biomater 4:318–323. https://doi.org/10.1016/j.actbio.2007.08.005
97. Tsuchiya H, Nakata J, Fujimoto S, Berger S, Schmuki P (2008) Anodic porous and tubular oxide layers on Ti alloys. In: ECS transactions. The Electrochemical Society, pp 359–367
98. Sieber I, Kannan B, Schmuki P (2005) Self-assembled porous tantalum oxide prepared in H2so 4/HF electrolytes. Electrochem Solid-State Lett 8:J10. https://doi.org/10.1149/1.1859676
99. Wei W, Macak JM, Schmuki P (2008) High aspect ratio ordered nanoporous Ta2O5 films by anodization of Ta. Electrochem Commun 10:428–432. https://doi.org/10.1016/j.elecom.2008.01.004
100. Oh S-H, Finõnes RR, Daraio C, Chen L-H, Jin S (2005) Growth of nano-scale hydroxyapatite using chemically treated titanium oxide nanotubes. Biomaterials 26:4938–4943. https://doi.org/10.1016/j.biomaterials.2005.01.048

101. Popat KC, Leoni L, Grimes CA, Desai TA (2007) Influence of engineered titania nanotubular surfaces on bone cells. Biomaterials 28:3188–3197. https://doi.org/10.1016/j.biomaterials.2007.03.020
102. Brammer KS, Oh S, Gallagher JO, Jin S (2008) Enhanced cellular mobility guided by TiO_2 nanotube surfaces 2008
103. Huo K, Gao B, Fu J, Zhao L, Chu PK (2014) Fabrication, modification, and biomedical applications of anodized TiO_2 nanotube arrays. RSC Adv 4:17300–17324
104. Indira K, Kamachi Mudali U, Rajendran N (2014) In vitro bioactivity and corrosion resistance of Zr incorporated TiO_2 nanotube arrays for orthopaedic applications. Appl Surf Sci 316:264–275. https://doi.org/10.1016/j.apsusc.2014.08.001
105. Xin Y, Jiang J, Huo K, Hu T, Chu PK (2009) Bioactive SrTiO3 nanotube arrays: Strontium delivery platform on Ti-based osteoporotic bone implants. ACS Nano 3:3228–3234. https://doi.org/10.1021/nn9007675
106. Indira K, Mudali UK, Rajendran N (2014) In-vitro biocompatibility and corrosion resistance of strontium incorporated TiO_2 nanotube arrays for orthopaedic applications. J Biomater Appl 29:113–129. https://doi.org/10.1177/0885328213516821
107. Simi VS, Kabali J, Rajendran N (2016) Development and characterization of zinc incorporated titania nanotube arrays for biomedical applications. Trends Biomater Artif Organs 29:286–293
108. Simi VS, Satish A, Korrapati PS, Rajendran N (2018) In-vitro biocompatibility and corrosion resistance of electrochemically assembled PPy/TNTA hybrid material for biomedical applications. Appl Surf Sci 445:320–334. https://doi.org/10.1016/j.apsusc.2018.03.151
109. Advanced biomaterials: fundamentals, processing, and applications. Wiley. https://www.wiley.com/en-us/Advanced+Biomaterials%3A+Fundamentals%2C+Processing%2C+and+Applications+-p-9780470193402. Accessed 22 Jun 2020
110. Fossati A, Borgioli F, Galvanetto E, Bacci T (2004) Corrosion resistance properties of plasma nitrided Ti–6Al–4 V alloy in nitric acid solutions. 46:917–927. https://doi.org/10.1016/S0010-938X(03)00188-4
111. Rudenja S, Leygraf C, Pan J, Kulu P, Talimets E, Mikli V (1999) Duplex TiN coatings deposited by arc plating for increased corrosion resistance of stainless steel substrates. Surf Coatings Technol 114:129–136. https://doi.org/10.1016/S0257-8972(99)00033-X
112. Strafford KN, Towell JM (1976) The interaction of titanium and titanium alloys with nitrogen at elevated temperatures. I. The kinetics and mechanism of the titanium-nitrogen reaction. Oxid Met 10:41–67. https://doi.org/10.1007/BF00611698
113. McDonald NR, Wallwork GR (1970) The reaction of nitrogen with titanium between 800 and 1200 °C. Oxid Met 2:263–283. https://doi.org/10.1007/BF00614621
114. Metin E, Inal OT (1989) Kinetics of layer growth and multiphase diffusion in ion-nitrided titanium. Metall Trans A 20:1819–1832. https://doi.org/10.1007/BF02663213
115. Mohan L, Anandan C, William Grips VK (2013) Investigation of electrochemical behavior of nitrogen implanted Ti-15Mo-3Nb-3Al alloy in Hank's solution. J Mater Sci Mater Med 24:623–633. https://doi.org/10.1007/s10856-012-4835-8
116. Mohan L, Anandan C (2013) Effect of gas composition on corrosion behavior and growth of apatite on plasma nitrided titanium alloy Beta-21S. Appl Surf Sci 268:288–296. https://doi.org/10.1016/j.apsusc.2012.12.080
117. Anandan C, Babu PD, Mohan L (2013) Effect of gas composition on nitriding and wear behavior of nitrided titanium alloy Ti-15 V-3Cr-3Al-3Sn. J Mater Eng Perform 22:2623–2633. https://doi.org/10.1007/s11665-013-0540-0
118. Mohan L, Raja MD, Uma TS, Rajendran N, Anandan C (2016) In-Vitro biocompatibility studies of plasma-nitrided titanium alloy β-21S using fibroblast cells. J Mater Eng Perform 25:1508–1514. https://doi.org/10.1007/s11665-015-1860-z
119. Anandan C, Mohan L (2016) Effect of PostNitride Annealing on Wear and Corrosion Behavior of Titanium Alloy Ti-6Al-4V. J Mater Eng Perform 25:4416–4424. https://doi.org/10.1007/s11665-016-2252-8
120. Mohan L, Anandan C, Rajendran N (2015) Effect of plasma nitriding on structure and biocompatibility of self-organised TiO_2 nanotubes on Ti–6Al–7Nb. RSC Adv 5:41763–41771. https://doi.org/10.1039/C5RA05818J

121. Mohan L, Dilli Babu P, Kumar P, Anandan C (2013) Influence of zirconium doping on the growth of apatite and corrosion behavior of DLC-coated titanium alloy Ti-13Nb-13Zr. Surf Interface Anal 45:1785–1791. https://doi.org/10.1002/sia.5323
122. Kumar P, Babu PD, Mohan L, Anandan C, Grips VKW (2012) Wear and corrosion behavior of Zr-doped DLC on Ti-13Zr-13Nb biomedical alloy. https://doi.org/10.1007/s11665-012-0230-3
123. Viswanathan S, Manjunath Reddy M, Mohan L, Bera P, Barshilia HC, Anandan C (2017) Corrosion and wear properties of Ti/tetrahedral amorphous carbon multilayered coating. J Bio- Tribo-Corrosion 3:39. https://doi.org/10.1007/s40735-017-0100-5
124. Viswanathan S, Mohan L, Bera P, Kumar VP, Barshilia HC, Anandan C (2017) Corrosion and wear behaviors of Cr-doped diamond-like carbon coatings. J Mater Eng Perform. https://doi.org/10.1007/s11665-017-2783-7
125. Viswanathan S, Mohan L, Chakraborty M, Mandal C, Bera P, Aruna ST, Anandan C (2018) Carbon plasma immersion ion implantation and DLC deposition on Ni–Ti alloy. Mater Manuf Process 33:1121–1127. https://doi.org/10.1080/10426914.2017.1415450
126. Viswanathan S, Mohan L, Bera P, Shanthiswaroop S, Muniprakash M, Barshilia HC, Anandan C (2018) Corrosion and wear resistance properties of multilayered diamond-like carbon nanocomposite coating. Surf Interface Anal 50:265–276. https://doi.org/10.1002/sia.6353
127. Gnanavel S, Ponnusamy S, Mohan L, Radhika R, Muthamizhchelvan C, Ramasubramanian K (2018) Electrochemical behavior of biomedical titanium alloys coated with diamond carbon in Hanks' solution. J Mater Eng Perform 27:1635–1641. https://doi.org/10.1007/s11665-018-3250-9
128. Wei Q, Narayan J (2000) Superhard diamondlike carbon: preparation, theory, and properties. Int Mater Rev 45:133–164. https://doi.org/10.1179/095066000101528340
129. Hauert R DLC Films in Biomedical Applications, pp 494–509
130. Mohan L, Viswanathan S, Anandan C, Rajendran N (2015) Corrosion behaviour of tetrahedral amorphous carbon (ta-C) filled titania nano tubes. RSC Adv 5:93131–93138. https://doi.org/10.1039/C5RA19625F
131. Shrestha NK, Macak JM, Schmidt-Stein F, Hahn R, Mierke CT, Fabry B, Schmuki P (2009) Magnetically guided titania nanotubes for site-selective photocatalysis and drug release. Angew Chemie—Int Ed 48:969–972. https://doi.org/10.1002/anie.200804429
132. Aw MS, Kurian M, Losic D (2013) Polymeric micelles for multidrug delivery and combination therapy. Chem—A Eur J 19:12586–12601. https://doi.org/10.1002/chem.201302097
133. Aw MS, Addai-Mensah J, Losic D (2012) A multi-drug delivery system with sequential release using titania nanotube arrays. Chem Commun 48:3348–3350. https://doi.org/10.1039/c2cc17690d
134. Simovic S, Diener KR, Bachhuka A, Kant K, Losic D, Hayball JD, Brownc MP, Vasilev K (2014) Controlled release and bioactivity of the monoclonal antibody rituximab from a porous matrix: a potential in situ therapeutic device. Mater Lett 130:210–214. https://doi.org/10.1016/j.matlet.2014.05.110
135. Mohan L, Anandan C, Rajendran N (2016) Drug release characteristics of quercetin-loaded TiO2 nanotubes coated with chitosan. Int J Biol Macromol 93:1633–1638. https://doi.org/10.1016/j.ijbiomac.2016.04.034